NASA TECHNICAL NOTE

NASA TN D-4843

NASA TN D-4843

TRANSONIC AERODYNAMIC CHARACTERISTICS OF POWERED MODELS OF SEVERAL APOLLO LAUNCH-ESCAPE VEHICLE CONFIGURATIONS

by Bobby Lee Berrier and Odis C. Pendergraft, Jr.

Langley Research Center
Langley Station, Hampton, Va.

NATIONAL AERONAUTICS AND SPACE ADMINISTRATION • WASHINGTON, D. C. • OCTOBER 1968

TRANSONIC AERODYNAMIC CHARACTERISTICS OF POWERED MODELS OF SEVERAL APOLLO LAUNCH-ESCAPE VEHICLE CONFIGURATIONS

By Bobby Lee Berrier and Odis C. Pendergraft, Jr.

Langley Research Center
Langley Station, Hampton, Va.

NATIONAL AERONAUTICS AND SPACE ADMINISTRATION

For sale by the Clearinghouse for Federal Scientific and Technical Information
Springfield, Virginia 22151 – CFSTI price $3.00

TRANSONIC AERODYNAMIC CHARACTERISTICS OF POWERED MODELS OF SEVERAL APOLLO LAUNCH-ESCAPE VEHICLE CONFIGURATIONS

By Bobby Lee Berrier and Odis C. Pendergraft, Jr.
Langley Research Center

SUMMARY

An investigation of several models of Apollo launch-escape vehicle configurations has been made at Mach numbers from 0.70 to 1.30. The effects of command module strakes, a flow separation device, escape-rocket tower modifications, nozzle cant angle, and offset thrust vector were investigated. The escape-rocket exhaust was simulated with a hydrogen peroxide rocket mounted upstream of the command module. The angle-of-attack range was -5° to 31°, and the average Reynolds number based on the maximum command-module diameter was 4.34×10^6 at a Mach number of 0.90.

The results of the investigation indicate that axial force (drag) was decreased because of favorable jet interference by adding strakes to the command module, by using a "ring-attachment" type of escape-rocket tower, or by increasing nozzle cant angle.

INTRODUCTION

Several investigations have been made of the aerodynamic characteristics of proposed Apollo launch-escape vehicle configurations. (See refs. 1 to 3.) All these investigations were made without simulation of the jet exhaust from the escape-rocket nozzles. An investigation of Mercury escape configurations with airflow through the rocket nozzles indicated that the aerodynamic characteristics were affected by escape-rocket exhaust flow. (See ref. 4.) Exhaust interference effects were also shown by later investigations on the Apollo launch-escape vehicle which utilized hydrogen peroxide decomposition products for hot exhaust gas simulation. (See refs. 5 and 6.)

The objective of the present investigation was to examine the jet interference effects on the aerodynamic characteristics of several modifications to the 0.085-scale model Apollo launch-escape vehicle used in references 5 and 6. The modifications consisted of addition of lateral strakes and a flow separator disk, two tower types, nozzle cant angles, and an offset thrust vector.

The tests were conducted in the Langley 16-foot transonic tunnel at Mach numbers from 0.70 to 1.30 at angles of attack from -5° to 31° over a thrust-coefficient range from

0 to 3.54. The test Reynolds number based on a model base diameter of 33.25 centimeters and free-stream conditions varied from 2.95×10^6 to 4.38×10^6.

SYMBOLS

The positive direction of forces and moments is shown in figure 1. The basic data presented herein are referred to the body system of axes with the origin located at the theoretical apex of the command module.

A	reference area, maximum cross-sectional area of command module, 868.2331 sq cm
d	maximum diameter of command module, 33.25 cm
l	length of command module measured from the theoretical apex, 30.78 cm
M	free-stream Mach number
p	pressure, N/m^2
q	dynamic pressure, N/m^2
α	angle of attack of model center line, deg
β	angle between model center line and nozzle center line, deg
ϕ	angular location with respect to module longitudinal axis positive in counterclockwise direction looking upstream, deg
θ	angle between model center line and thrust axis, deg

Subscripts:

a	ambient
f	static thrust
j	jet

t total

∞ free stream

Aerodynamic coefficients (include jet-interference effects but not the direct forces or moments produced by the jet):

C_A axial-force coefficient, $\frac{\text{Axial force}}{q_\infty A}$

C_m pitching-moment coefficient, $\frac{\text{Pitching moment}}{q_\infty Ad}$

C_N normal-force coefficient, $\frac{\text{Normal force}}{q_\infty A}$

Coefficients of force and moment components of jet thrust:

$C_{A,f}$ static axial-thrust coefficient, $\frac{(\text{Axial force})_j}{p_a A}$

$C_{A,j}$ thrust coefficient, $\frac{(\text{Axial force})_j}{q_\infty A \cos \beta}$

C_j resultant thrust coefficient, $\frac{C_{A,f}}{\cos \theta}$ or $\frac{C_{A,j} \cos \beta}{\cos \theta}$

$C_{m,f}$ static pitching-moment coefficient, $\frac{(\text{Pitching moment})_j}{p_a Ad}$

$C_{m,j}$ pitching-moment coefficient, $\frac{(\text{Pitching moment})_j}{q_\infty Ad}$

$C_{N,f}$ static normal-force coefficient, $\frac{(\text{Normal force})_j}{p_a A}$

$C_{N,j}$ normal-force coefficient, $\frac{(\text{Normal force})_j}{q_\infty A}$

Coefficients with aerodynamic and thrust components included:

$C_{A,t}$ total axial-force coefficient, $C_A - C_{A,j} \cos \beta$

$C_{m,t}$ total pitching-moment coefficient, $C_m + C_{m,j}$

$C_{N,t}$ total normal-force coefficient, $C_N + C_{N,j}$

APPARATUS AND PROCEDURE

Wind Tunnel

The present investigation was conducted in the Langley 16-foot transonic tunnel, which is a single-return, atmospheric wind tunnel with an octagonal test section and continuous air exchange. The tunnel has a continuously variable speed range from a Mach number of 0.20 to 1.30.

Model and Support System

A sketch of the Apollo launch-escape vehicle and sting support is shown in figure 2. The model consisted of the escape-rocket simulator, rocket-support structure, and the command module. Additional model details and configuration code designations are given in figure 3. Photographs of several model configurations installed in the test section of the Langley 16-foot transonic tunnel are shown in figure 4.

Command module.- The command module was investigated without and with the antenna housings and umbilical fairing. These configurations are designated C1 and C2, respectively, and are shown in figure 3(a). In addition, figure 3(a) shows two strake configurations designated C3 and C4. The strakes were located in the yaw plane and their function was to eliminate unwanted trim points in pitch that occurred for the command module alone. (See ref. 7.) However, since the command module was not investigated without the escape-rocket structure in the present investigation, the objective of this investigation was to determine the effect of the strakes on the aerodynamic characteristics of a powered model of the entire launch-escape vehicle at low angles of attack.

Escape-rocket tower structure.- Two different escape-rocket tower structures were investigated to determine their effect on the aerodynamic characteristics of the Apollo launch-escape vehicle. Details of the two tower structures are given in figure 3(b). Both towers had four longitudinal members. The diagonal members in the first bay of the tower designated T1 were connected to a ring perpendicular to the tower center line and located slightly inside the four longitudinal members. This tower (T1) is referred to as the "ring attachment" type. The tower designated T2 had diagonal members which were connected directly to the longitudinal members and did not project into the inside volume of the tower structure. This tower (T2) is referred to as the "side attachment" type.

Escape rocket.- Figure 3(c) presents a sketch of the two escape-rocket configurations of the investigation. Both escape-rocket configurations were identical except for a collar and 14.034-cm-diameter disk (flow separator) added around the rocket skirt for the configuration designated R2 and intended as a solution to dynamic stability problems

of the launch-escape vehicle. (See ref. 8.) However, the objective of the present investigation was to determine the effect of the disk on the static longitudinal aerodynamic characteristics only.

Nozzles.- The sketch and table shown in figure 3(d) give details of the four sets of nozzle configurations. Nozzle cant angles of 21°, 35°, and 42° (designated N1, N2, and N3, respectively) were used to study the effect of nozzle cant angle. The throat and exit areas of all the nozzles for these configurations were the same and thus produced a thrust vector along the model center line ($\theta = 0^{\circ}$). In order to determine the effect of an offset thrust vector on the aerodynamic characteristics of the launch-escape vehicle, a fourth set of nozzles (designated N4) with unequal throat areas in the pitch plane was investigated. The resultant thrust vector ($\theta = 2^{\circ}45'$) produces a pitching moment intended to curve the launch-escape vehicle flight path away from the booster.

Exhaust simulation.- The escape-rocket exhaust flow was simulated by the hydrogen peroxide gas generator shown in figure 5. A more detailed description of the catalyst pack, escape rocket, and propellant-supply system may be found in reference 5. Typical hydrogen peroxide hot-jet simulators and the related propellant-supply system are described in reference 9. The four longitudinal members of the escape-rocket tower structure were used to pipe liquid hydrogen peroxide into a radial-flow catalyst pack located in the escape rocket. A flexible helix restraint system was used to pass the propellant lines over the balance so that restraint on the balance was held to a minimum. (See ref. 5.) The resulting exhaust products of rocket-motor operation – oxygen and superheated steam (1011° K) – were exhausted through four nozzles located at the rocket base and canted outward at an angle β. The model rocket nozzles had scaled throat and exit areas and the same expansion ratios as the full-scale rocket nozzles. The two nozzles in the yaw plane had equal exit area to throat area ratios of 8.59 for all the configurations of the investigation. The top and bottom nozzles in the pitch plane had exit area to throat area ratios of 10 and 7.62, respectively, for the configuration utilizing the N4 nozzle set. The asymmetric thrust of the pitch nozzles provided the offset thrust vector ($2^{\circ}45'$) shown in figure 1 only for the N4 nozzles ($\theta = 0^{\circ}$ for N1, N2, and N3 nozzle sets).

Instrumentation

Forces and moments on the model were measured by a six-component strain-gage balance. Liquid hydrogen peroxide flow rate was measured with a vane type of electronic flowmeter located in the hydrogen peroxide supply line. Rocket-exhaust plenum chamber pressures were measured at the locations indicated in figure 5. The signals from the balance, pressure transducers, and the flowmeter were converted to dc millivolts and recorded on magnetic tape.

Tests

The present investigation covered a Mach number range from 0.70 to 1.30 and angles of attack from -5° to 31°. Thrust coefficient $C_{A,j}$ was varied from 0 to about 3.54 depending upon Mach number. The average Reynolds number based on the maximum command-module base diameter was 4.34×10^6 at a Mach number of 0.90.

The test runs were made by first setting the Mach number and angle of attack and then taking data through a range of chamber-pressure ratios from 1 (jets off) to the maximum. In the course of operating the rocket through the cycle, the tunnel Mach number varied somewhat, particularly at supersonic speeds. For example, where data are presented at a nominal value of $M = 1.3$, some of the test points may actually be at Mach numbers that are as low as 1.28. In addition, chamber pressure varied slightly from the values desired and hence could not be duplicated at each angle of attack for a given Mach number. Therefore, the data are also presented at nominal values of thrust coefficient.

DATA REDUCTION

Standard force coefficients were obtained from millivolt readings by machine computation. All aerodynamic coefficients, except where noted, in this report have all applicable components of the jet thrust removed as follows:

$$C_A = C_{A,t} + C_{A,j} \cos \beta$$

$$C_m = C_{m,t} - C_{m,j}$$

$$C_N = C_{N,t} - C_{N,j}$$

This calculation removes all force and moment components due to jet thrust but retains all jet-exhaust interference effects on the command-module aerodynamic characteristics.

The components of axial force $C_{A,f}$, normal force $C_{N,f}$, and pitching moment $C_{m,f}$ due to the rocket thrust were obtained from a static calibration. Static rocket-thrust calibrations were conducted with a shroud around the command module, which was not attached to the balance, to prevent measurement of any jet interference forces on the module. The variation of $C_{A,f}$, $C_{N,f}$, and $C_{m,f}$ with rocket-chamber pressure ratio is presented in figure 6. The jet-thrust coefficient was obtained from the static calibrations as follows:

$$C_{A,j} = \frac{(\text{Axial force})_j}{q_\infty A \cos \beta} \quad \text{or} \quad \frac{(\text{Axial force})_j}{p_a A \cos \beta}$$

A static calibration of the 21° nozzle set was not made because of excessive impingement of hot gas on the command module. The calibration curve given in figure 6(a) for the 21° nozzle set was obtained by normalizing both slope and intercept for

the other three sets of nozzles (N2, N3, and N4) by dividing by the cosine of the cant angle. The average slope and intercept thus obtained were multiplied by cosine of 21° to give the line shown. Since the thrust vectors of the N1, N2, and N3 nozzles were symmetric to the center line of the model, the normal-force and pitching-moment coefficients were essentially zero and are not shown in figures 6(b) and 6(c) for these nozzle configurations.

RESULTS AND DISCUSSION

The effects of escape-rocket operation and angle of attack on the static aerodynamic characteristics of configuration C2-T1-R1-N2 are well documented in reference 5. Since similar results were obtained for all configurations of this investigation, these effects will not be discussed here but can be readily deduced from the figures presented. The present paper merely describes the effect of configuration modifications on the aerodynamic characteristics including jet interference effects.

Effect of Command-Module Strakes

The effect of command-module strakes on force and moment coefficients is shown in figure 7. The variation of axial-force coefficient with angle of attack is presented in figure 7(a). The addition of strakes to the command module in the yaw plane had little effect on axial-force coefficient for the $C_{A,j} = 0$ case except at low angles of attack and $M = 1.00$ where the addition of the "two-piece" strake (C3) decreased the axial force (drag) slightly. With the escape rocket operating, the addition of either strake configuration (C3 or C4) decreased axial force (drag) by reducing adverse jet interference effects. The two-piece strake generally gave the lowest axial-force coefficient except at $M = 1.28$, $C_{A,j} = 0.81$.

Because of the increased planform area, normal force increased for $\alpha > 0$ and decreased for $\alpha < 0$ for most test conditions when either strake configuration was added to the command module as shown in figure 7(b). Little effect is shown at low angles of attack for the jet-off case.

Figure 7(c) presents the variation of pitching-moment coefficient with angle of attack for several values of Mach number and thrust coefficient. Addition of the two-piece strake (C3) had no effect on pitching moment at low angles of attack for the jet-off case; however, at higher angles of attack, addition of the two-piece strake (C3) increased stability for $M = 1.00$ and shifted the unstable pitch-up condition at $M = 1.28$ from approximately 8° to 11°. For jet-on conditions, the addition of the C3 strakes increased stability for $20^{\circ} < \alpha < 31^{\circ}$ at $M = 1.00$ whereas no definite trend is shown at $M = 1.28$.

Addition of the one-piece strake (C4) had little effect on stability in the angle-of-attack range investigated except at $M = 1.00$, $C_{A,j} = 2.3$ where the unstable pitch-up condition was eliminated.

Effect of Escape-Rocket Tower Modification

Figure 8 presents the effect of escape-rocket tower modifications on the jet-off aerodynamic characteristics of the launch-escape vehicle. Modification of the escape rocket from the side attachment type (T2) to the ring attachment type (T1) decreased axial force (drag) at most test conditions. Increasing Mach number decreased this favorable effect until at $M = 1.27$, the axial-force coefficient for the (T1) type tower was slightly higher than that for the side attachment type (T2). Little or no effect of tower modification was found on jet-off normal-force and pitching-moment coefficients as shown in figures 8(b) and 8(c).

Effect of Rocket Skirt Disk

The effect of a flow separator disk on the aerodynamic characteristics of the launch-escape vehicle is shown in figure 9. The flow separator was intended as a dynamic stability fix for problems found in other investigations. (See ref. 8.) For jet-off conditions, mixed results were obtained by adding the disk to the escape rocket; axial force (drag) was generally decreased at $M = 1.00$ and $M = 1.26$ but was increased at $M = 0.70$, as shown in figure 9(a). An unfavorable increase of axial force is shown in figure 9(a) for the disk configuration when the escape rocket is operating.

For jet-off conditions, addition of the disk increased the absolute value of normal-force coefficient throughout the range of test conditions as shown in figure 9(b). The effect of the disk on normal force was small and erratic for jet-on conditions.

The jet-off longitudinal static stability was increased by the addition of the disk for $-5^{\circ} < \alpha < 8^{\circ}$ as shown in figure 9(c). The unstable pitch up shown for jet-off conditions at $M = 1.26$ was shifted from approximately 10° to 12°. The jet-on data were more erratic than the jet-off data but several instances of stability increases may be noted.

Effect of Nozzle Cant Angle

The effect of nozzle cant angle on the Apollo launch-escape vehicle aerodynamic characteristics is shown in figure 10. The data shown in figure 10 are plotted for a constant nominal value of $C_{A,j} \cos \beta$ (propulsive or axial component of thrust, see fig. 1) rather than $C_{A,j}$ since it was desired to determine the effects of nozzle cant angle at equal net axial force and not equal net nozzle thrust.

Nozzle cant angle had little or no effect on axial-force coefficient for jet-off conditions. Axial force (drag) was greatly reduced by increasing nozzle cant angle when the

escape rocket was operating. This favorable decrease of axial force is probably caused by less exhaust impingement on the command module surface when the 35^{o} and 42^{o} cant angle nozzles are utilized. At $M = 0.70$, the 35^{o} and 42^{o} cant angle nozzles give approximately the same axial-force level. With increasing Mach number, however, the jet-exhaust stream is turned so that the 35^{o} cant angle nozzle has a higher axial-force (drag) level because of exhaust impingement than the 42^{o} cant angle nozzle.

Little or no effect of nozzle cant angle on normal force is shown in figure 10(b). Some erratic variations due to rocket exhaust flow is shown for the jet-on conditions.

Nozzle cant angle had little effect on pitching-moment coefficient for jet-off conditions as shown in figure 10(c). Generally erratic behavior of pitching moment is observed for the jet-on case. However, it can be seen that the 42^{o} nozzle cant angle produced an unstable condition at $M = 0.70$ and the 21^{o} nozzle cant angle configuration became unstable at a lower angle of attack than the 35^{o} nozzle cant angle at $M = 1.28$.

Effect of Offset Thrust Vector

Figure 11 presents the effect of an offset thrust vector on axial-force, normal-force, and pitching-moment coefficients. As might be expected, no effect of an offset thrust vector on axial force, normal force, or pitching moment is shown for the jet-off case. With the escape rocket operating, axial force is decreased slightly at low angles of attack for a thrust vector $\theta = 0^{o}$ as compared with $\theta = 2.45$. Little or no jet interference on normal force and pitching moment due to an offset thrust vector is shown for the jet-on case.

Total pitching-moment coefficient (includes component due to rocket thrust) is shown in figure 12 plotted against angle of attack for the jet-on case. As might be expected, an increase of thrust vector from 0^{o} to $2^{o}45'$ increases pitching moment. The general trends of the curves do not greatly change with thrust vector and this fact indicates a small effect of jet interference on the launch-escape vehicle as shown by figure 11.

CONCLUSIONS

An investigation of a 0.085-scale model of several Apollo launch-escape vehicle configurations including the effects of escape-rocket-exhaust interference has been conducted. The results of the investigation have led to the following conclusions:

1. Addition of strakes to command module in the yaw plane generally decreased jet-on axial force (drag), increased the absolute value of normal force and had mixed results on pitching moment.

2. The ring attachment type of rocket tower structure produced lower values of axial force (drag) than the side attachment type of tower for jet-off conditions except at a Mach number of 1.27. The tower modifications had little or no effect on normal force or pitching moment (jet-off).

3. Axial force (drag) was increased by the addition of the flow-separator disk at jet-on conditions whereas normal force and pitching moment did not exhibit any definite trends due to jet interference.

4. Increasing nozzle cant angle decreased the axial force (drag) for jet-on conditions and had mixed effects on normal force and pitching moment.

5. Although an offset thrust vector obtained by using different nozzle throat areas in the pitch plane increased the total pitching-moment coefficient, the effects of jet interference due to offset thrust on axial force, normal force, and pitching moment were negligible.

Langley Research Center,
National Aeronautics and Space Administration,
Langley Station, Hampton, Va., July 26, 1968,
124-07-02-02-23.

REFERENCES

1. Pearson, Albin O.: Wind-Tunnel Investigation of the Static Longitudinal Aerodynamic Characteristics of Models of Reentry and Atmospheric-Abort Configurations of a Proposed Apollo Spacecraft at Mach Numbers From 0.3 to 1.20. NASA TM X-604, 1961.

2. Pearson, Albin O.: Wind-Tunnel Investigation of the Static Longitudinal Aerodynamic Characteristics of a Modified Model of a Proposed Apollo Atmospheric-Abort Configuration at Mach Numbers From 0.30 to 1.20. NASA TM X-686, 1962.

3. Boisseau, Peter C.: Low-Speed Static and Oscillatory Stability Characteristics of a Model of the Apollo Launch-Escape Vehicle and Command Module. NASA TM X-894, 1963.

4. Johnson, Joseph L., Jr.: Wind-Tunnel Investigation at Low Subsonic Speeds of the Static and Oscillatory Stability Characteristics of Models of Several Space Capsule Configurations. NASA TM X-285, 1960.

5. Runckel, Jack F.; Schmeer, James W.; and Pendergraft, Odis C., Jr.: Static Longitudinal Aerodynamic Characteristics of a Powered Model Of The Apollo Launch-Escape Vehicle From Mach 0.50 to 1.30. NASA TM X-1215, 1966.

6. Berrier, Bobby L.; and Pendergraft, Odis C., Jr.: Transonic Aerodynamic Characteristics of a Powered Wind-Tunnel Model of the Apollo Launch-Escape Vehicle During Separation. NASA TM X-1336, 1967.

7. Malcolm, Gerald N.; and Kirk, Donn B.: Comparison of Free-Flight and Conventional Wind-Tunnel Stability Tests for Apollo Command Module and Abort Configurations. NASA TM X-1137, 1965.

8. Averett, Benjamin T.; and Wright, Bruce R.: Some Dynamic-Stability Characteristics of Models of Proposed Apollo Configurations at Mach Numbers From 1.60 to 2.75. NASA TM X-971, 1964.

9. Runckel, Jack F.; and Swihart, John M.: A Hydrogen Peroxide Hot-Jet Simulator for Wind-Tunnel Tests of Turbojet-Exit Models. NASA MEMO 1-10-59L, 1959.

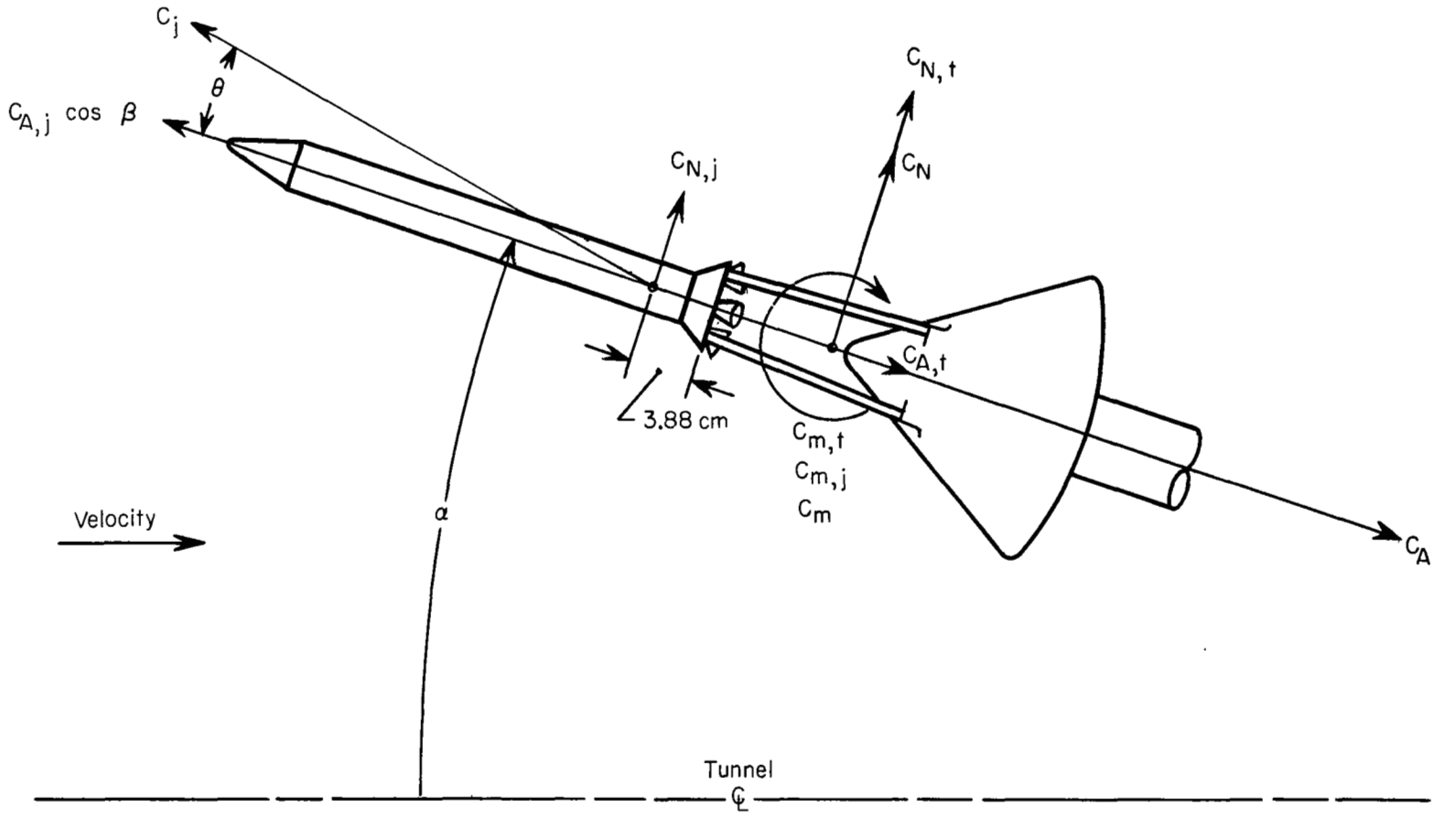

Figure 1.- Body system of axis. Force and moment coefficients on model including rocket thrust components. Arrows indicate positive direction.

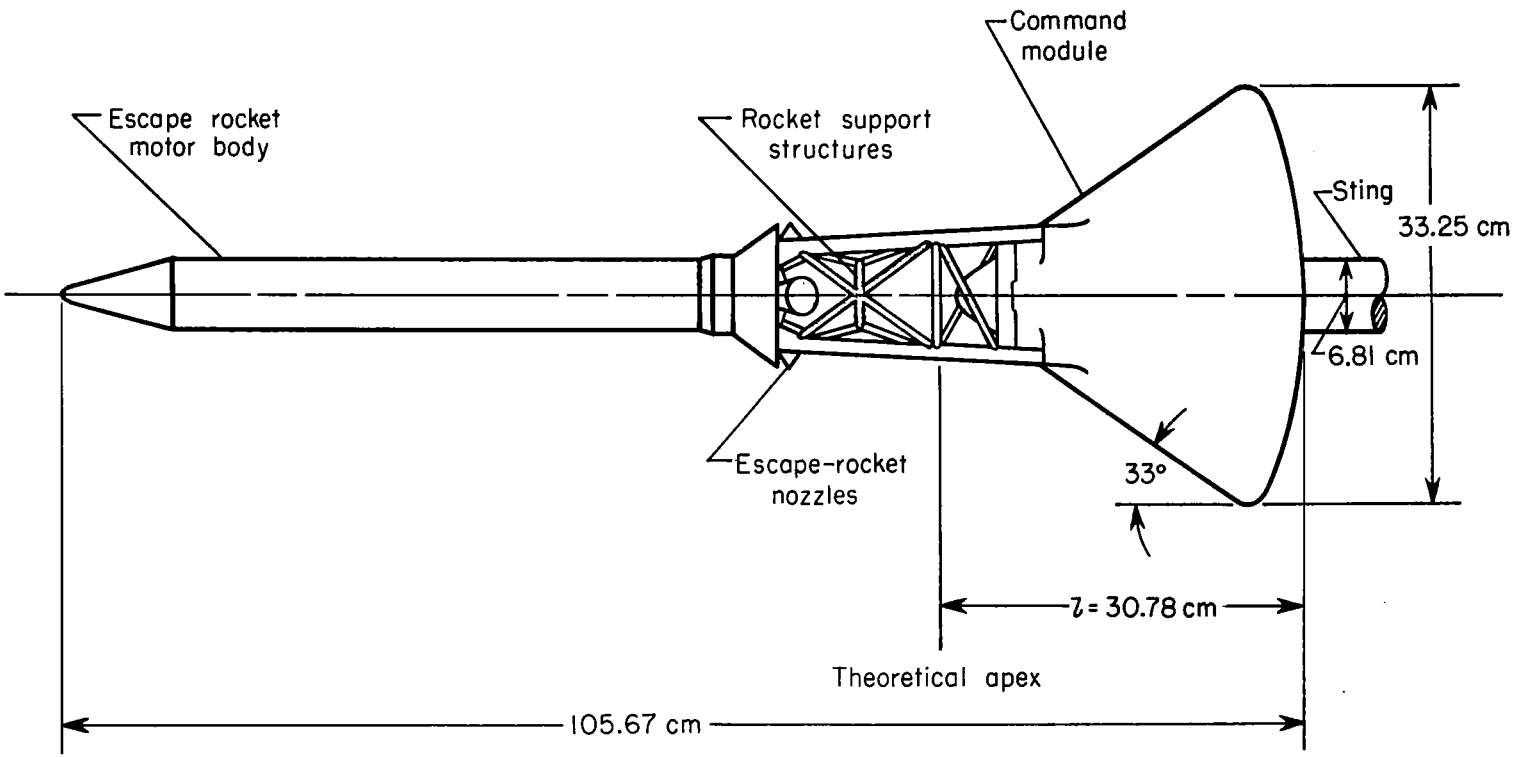

Figure 2.- Model sketch of Apollo launch-escape system.

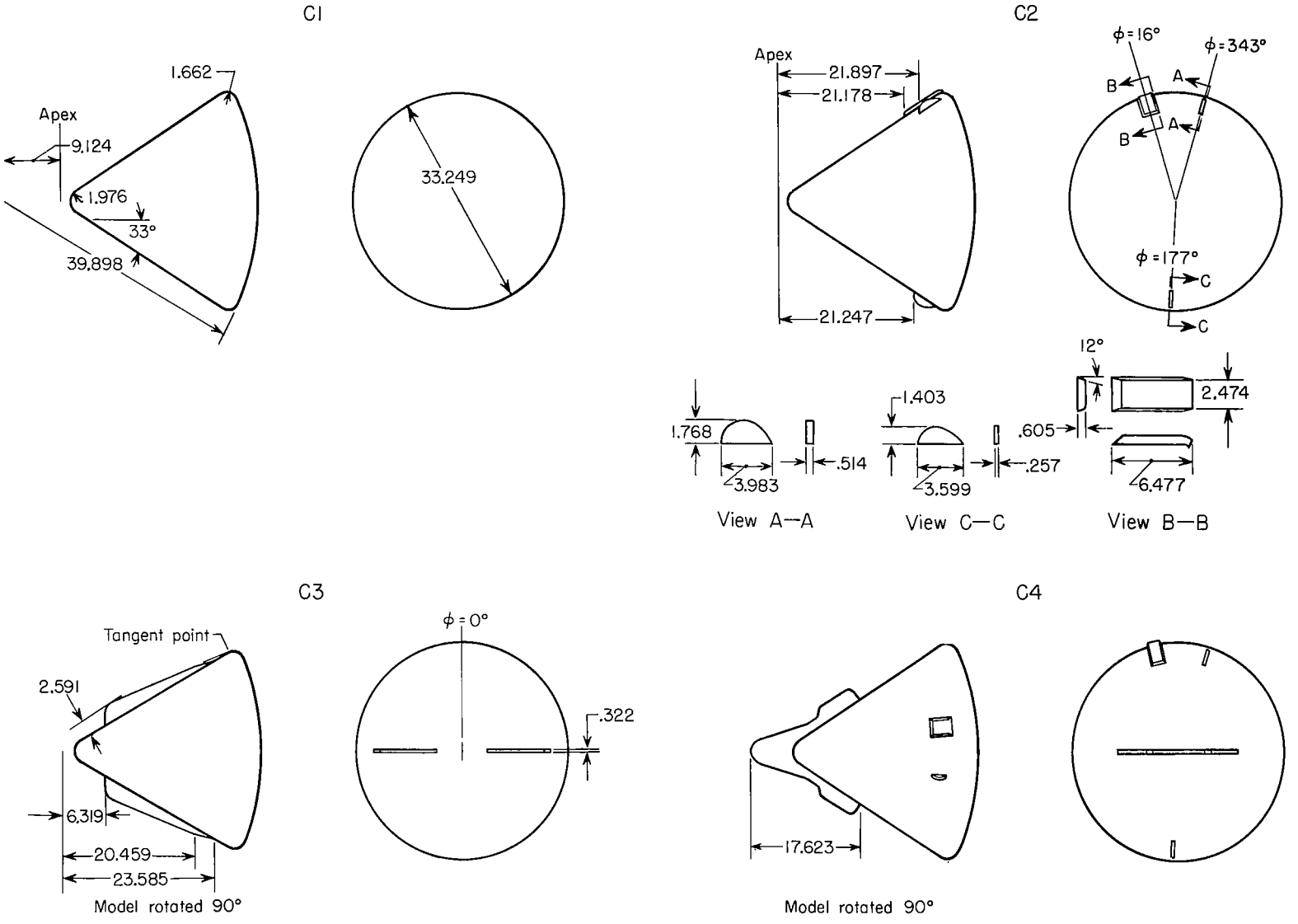

(a) Command module details.

Figure 3.- Sketch giving configuration details and configuration code. All dimensions are in centimeters.

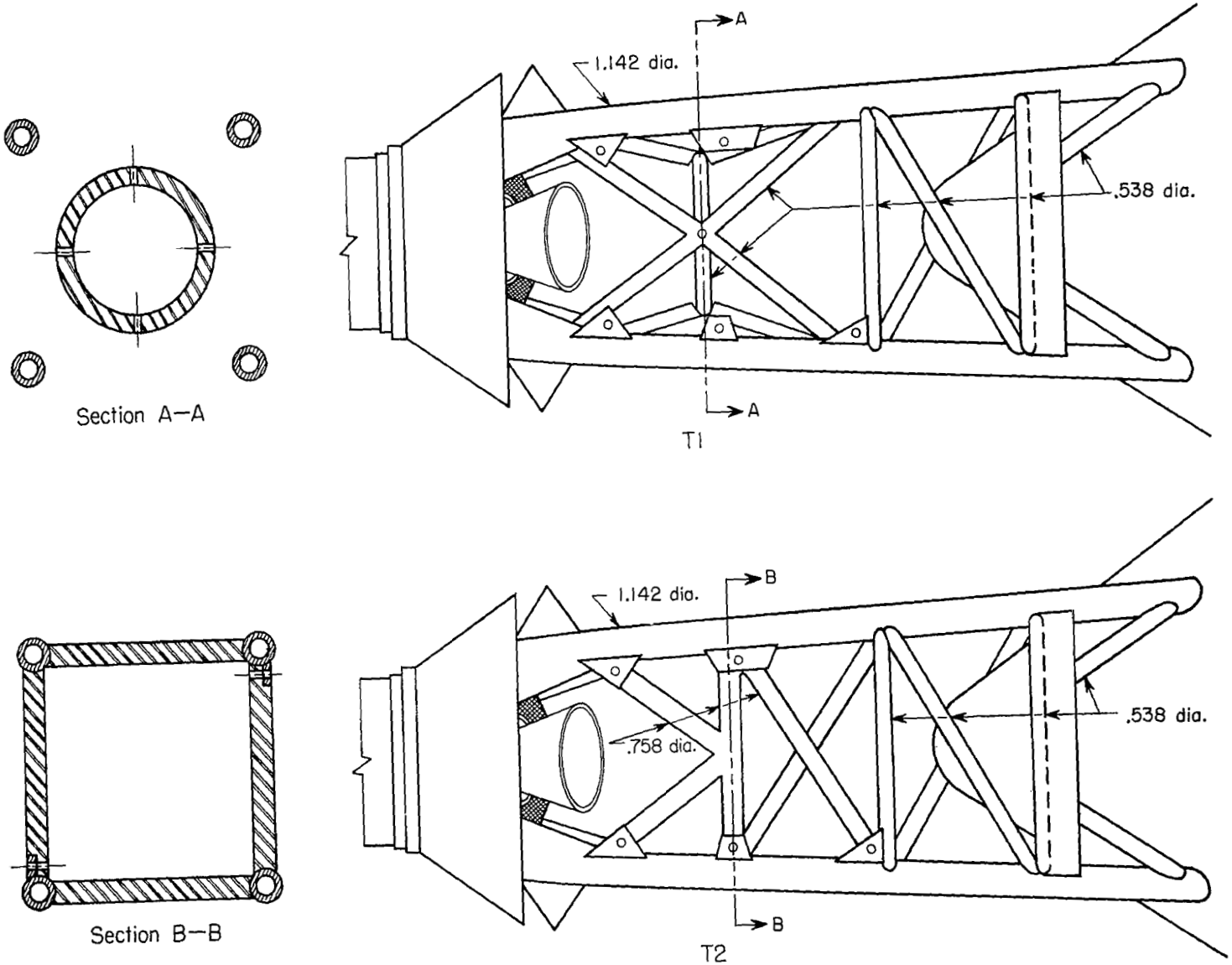

(b) Rocket tower details.

Figure 3 - Continued.

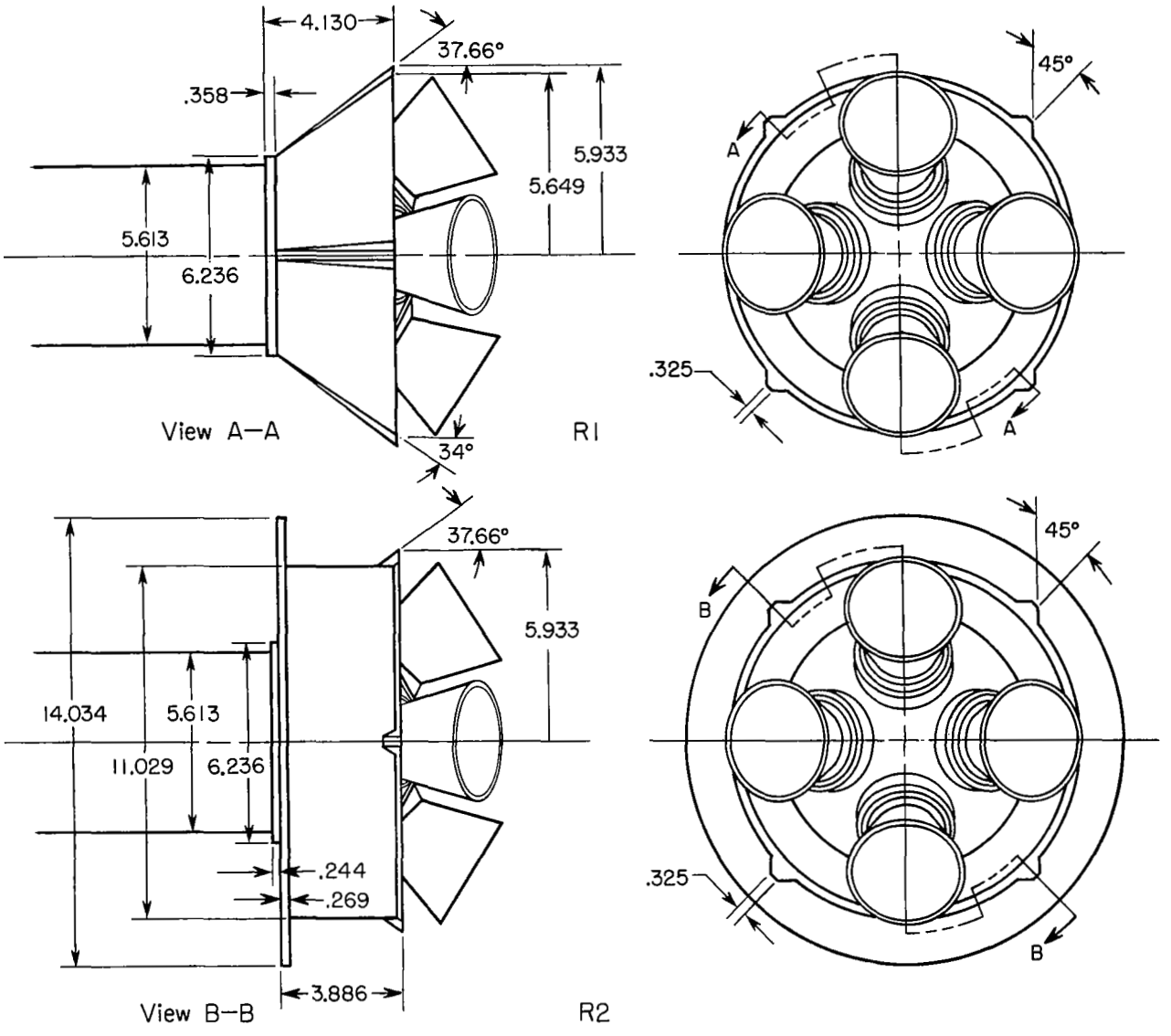

(c) Rocket skirt details.

Figure 3.- Continued.

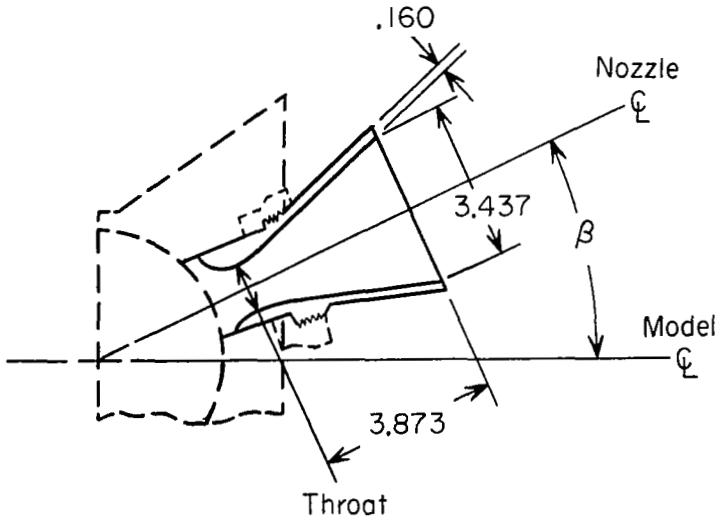

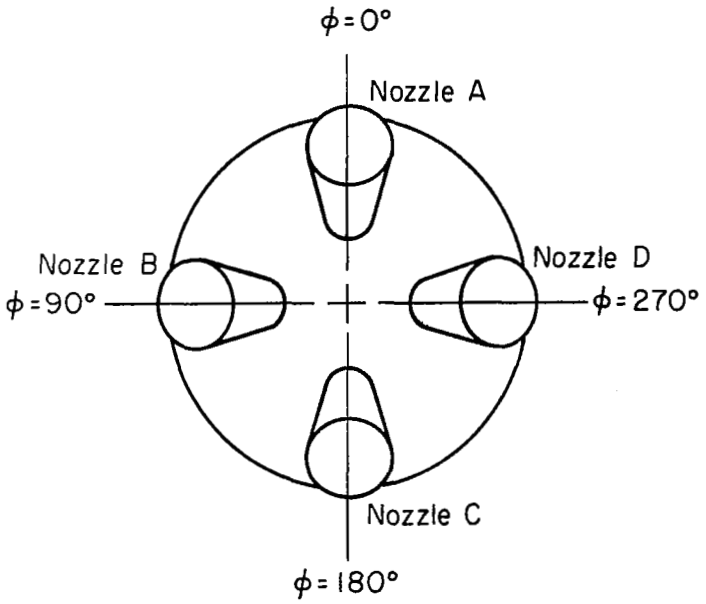

Nozzle set	β, deg	Throat diameter			
		Nozzle A	Nozzle B	Nozzle C	Nozzle D
N1	21	1.168	1.168	1.168	1.168
N2	35	1.168	1.168	1.168	1.168
N3	42	1.168	1.168	1.168	1.168
N4	35	1.084	1.168	1.246	1.168

(d) Rocket nozzle details.

Figure 3.- Concluded.

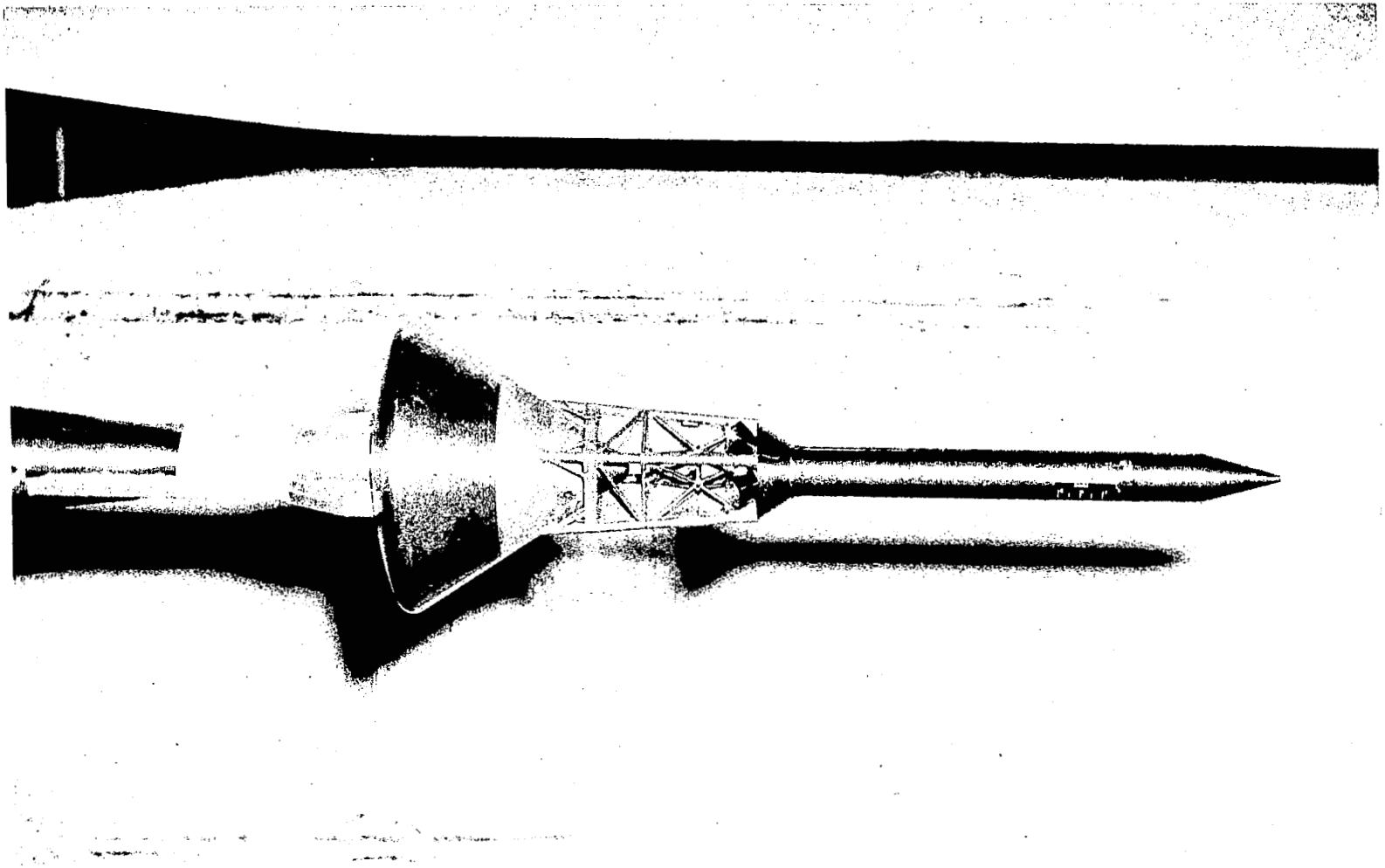

(a) Configuration C1-T1-R1-N2. L-62-8141

Figure 4.- Photograph of model installed in Langley 16-foot tunnel test section.

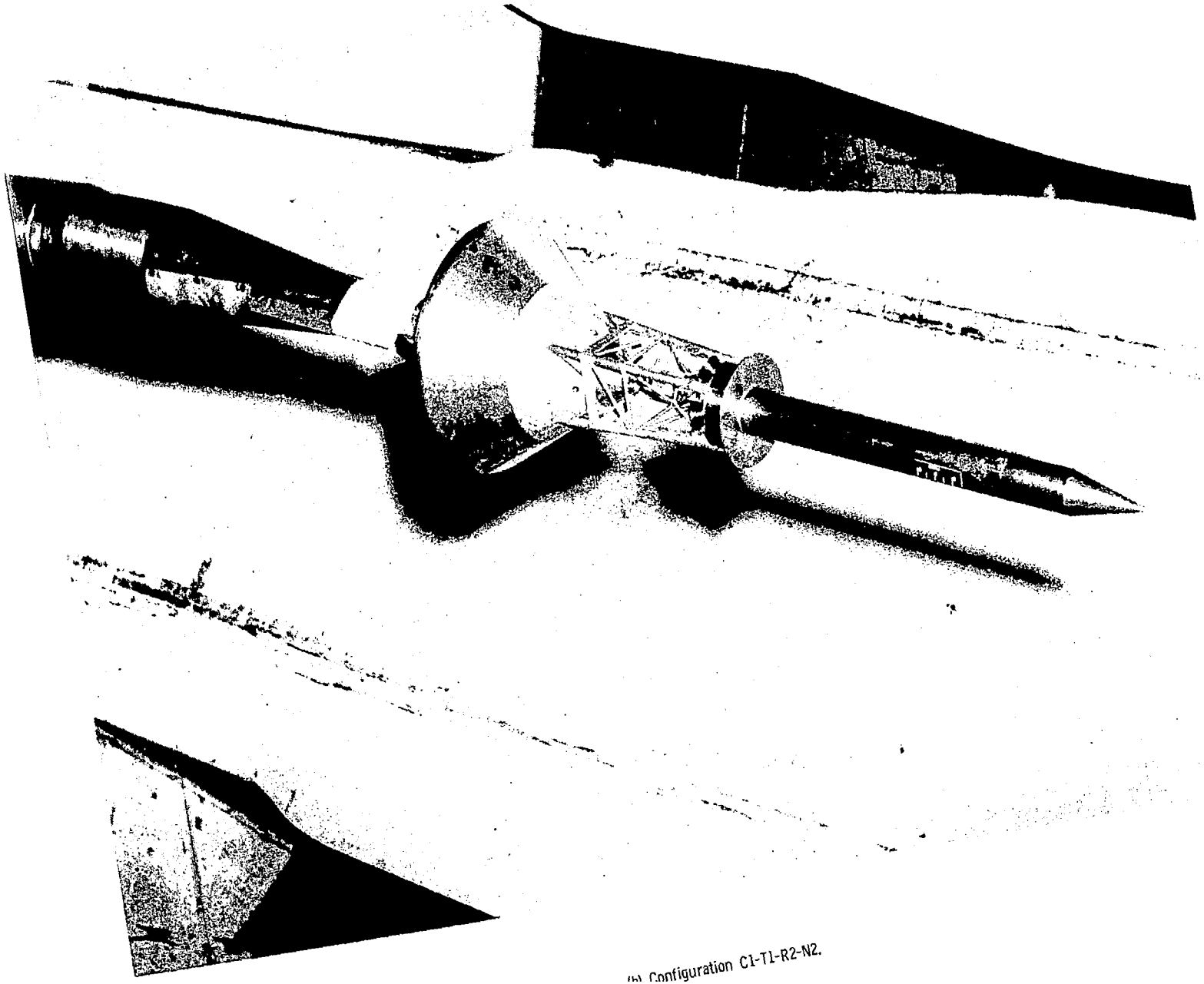

L-62-8142

(b) Configuration C1-T1-R2-N2.

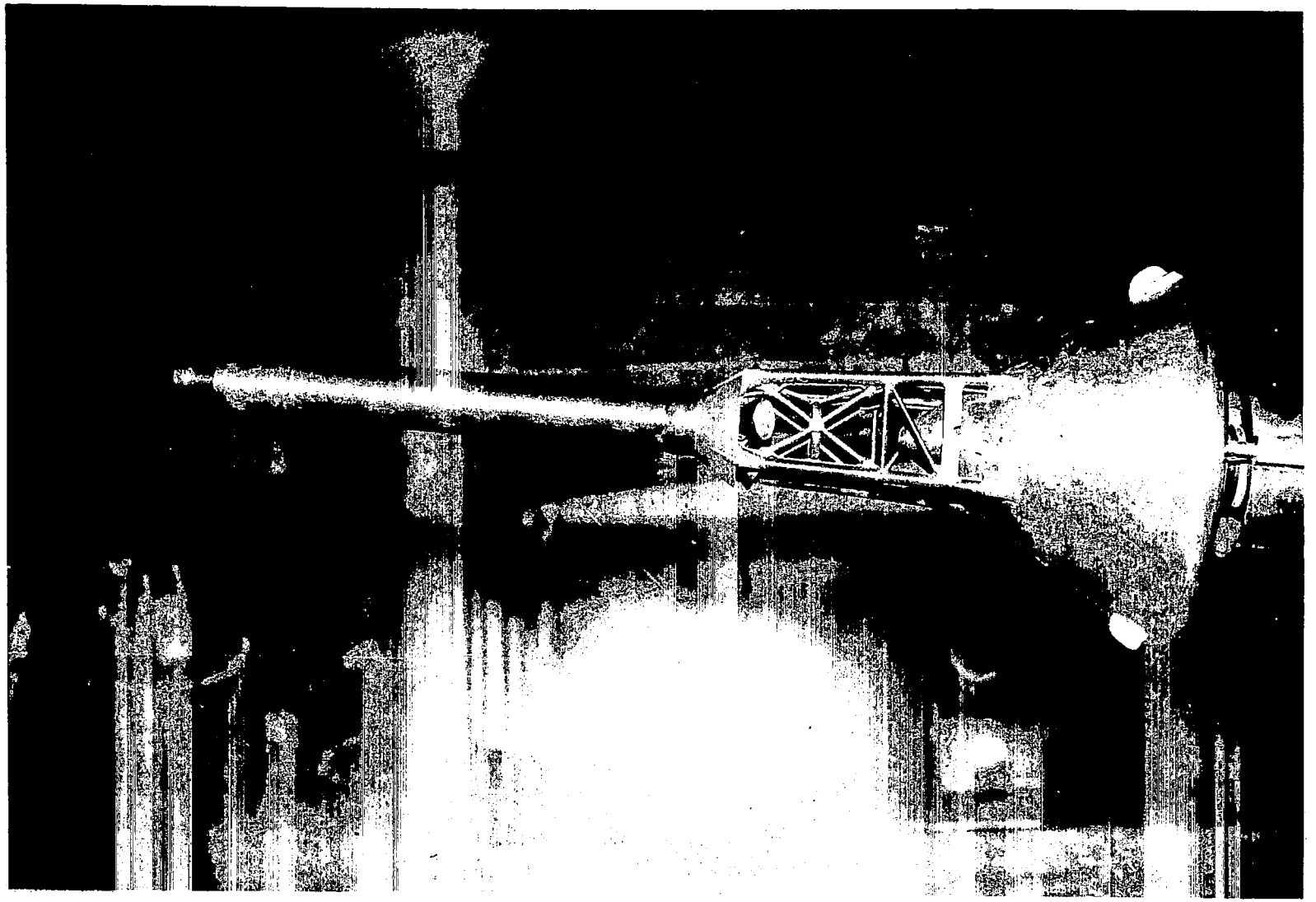

(c) Configuration C2-T1-R1-N2. L-64-2653

Figure 4.- Continued.

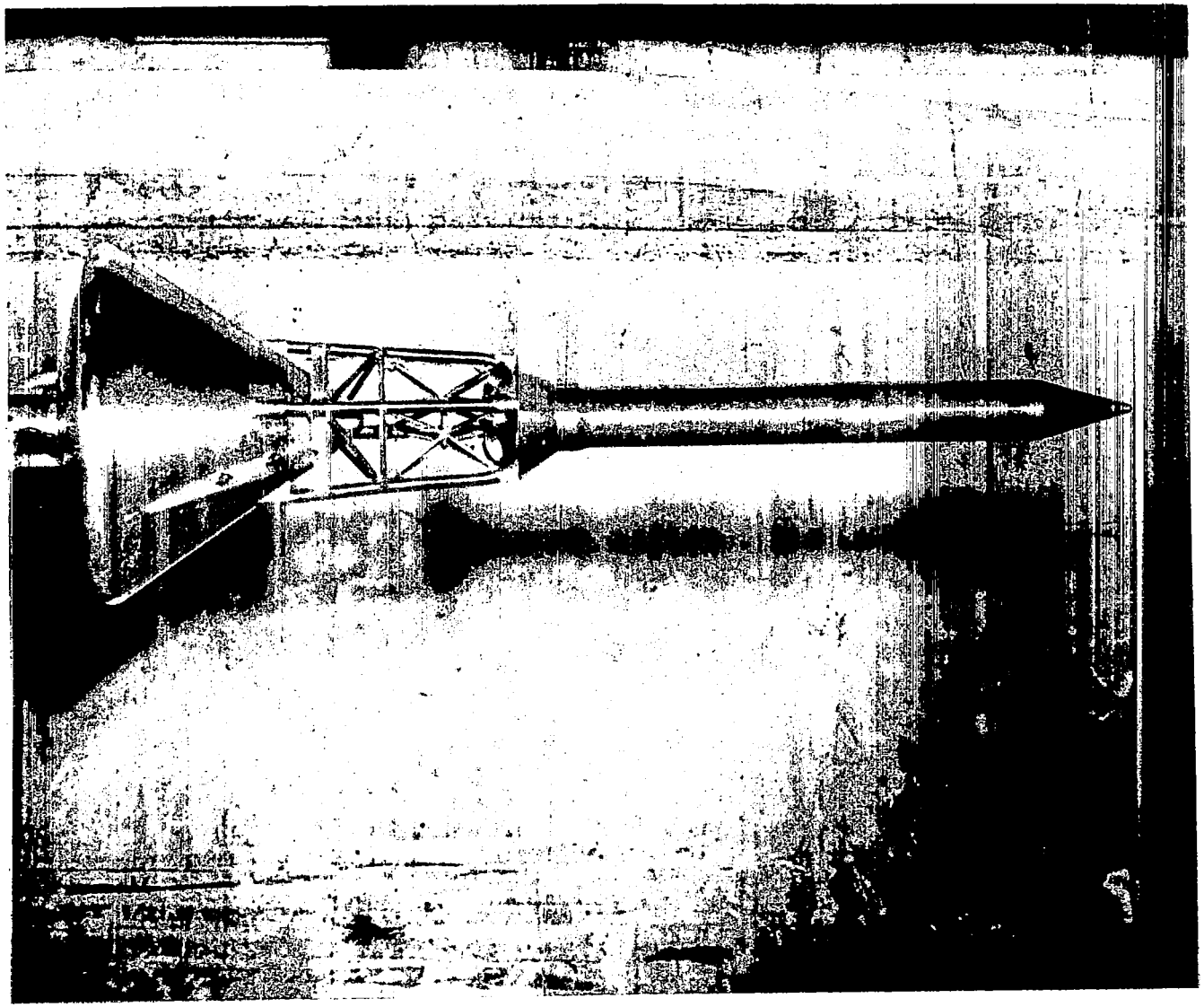

(d) Configuration C3-T1-R1-N2. L-63-2018

Figure 4.- Concluded.

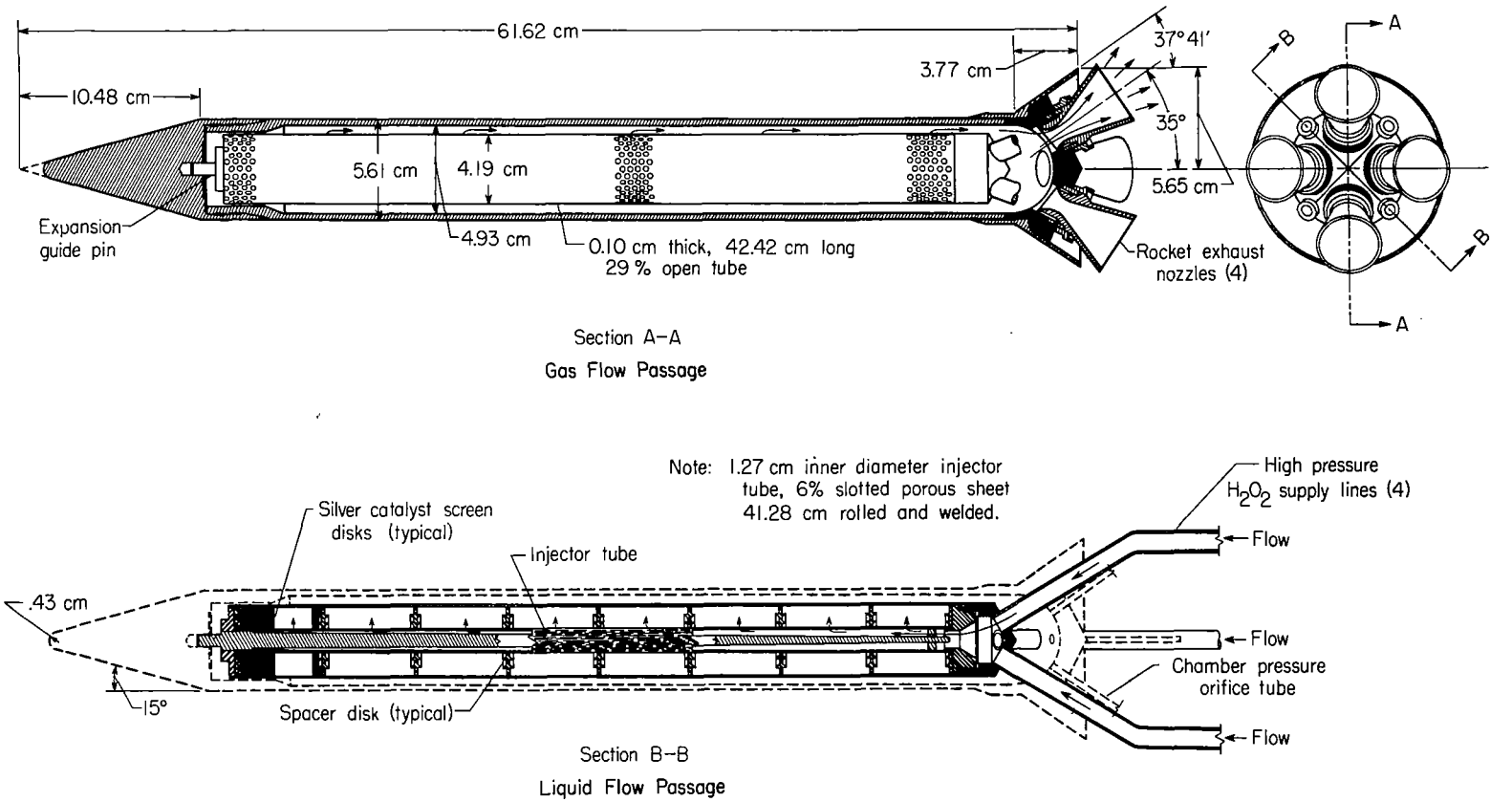

Figure 5.- Sketch of rocket decomposition chamber.

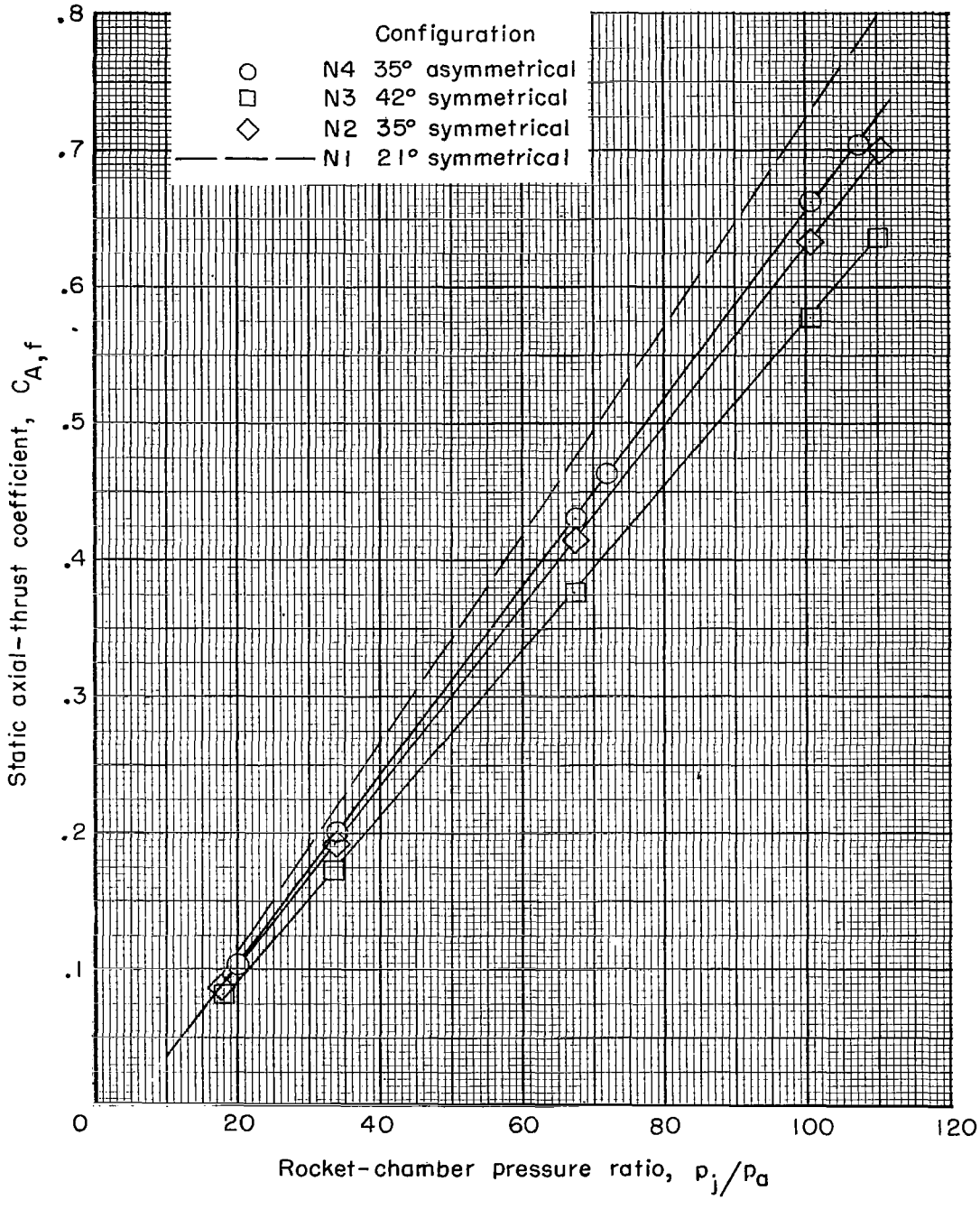

(a) Variation of axial-force coefficient with rocket-chamber pressure ratio.

Figure 6.- Static thrust calibrations of launch-escape vehicle.

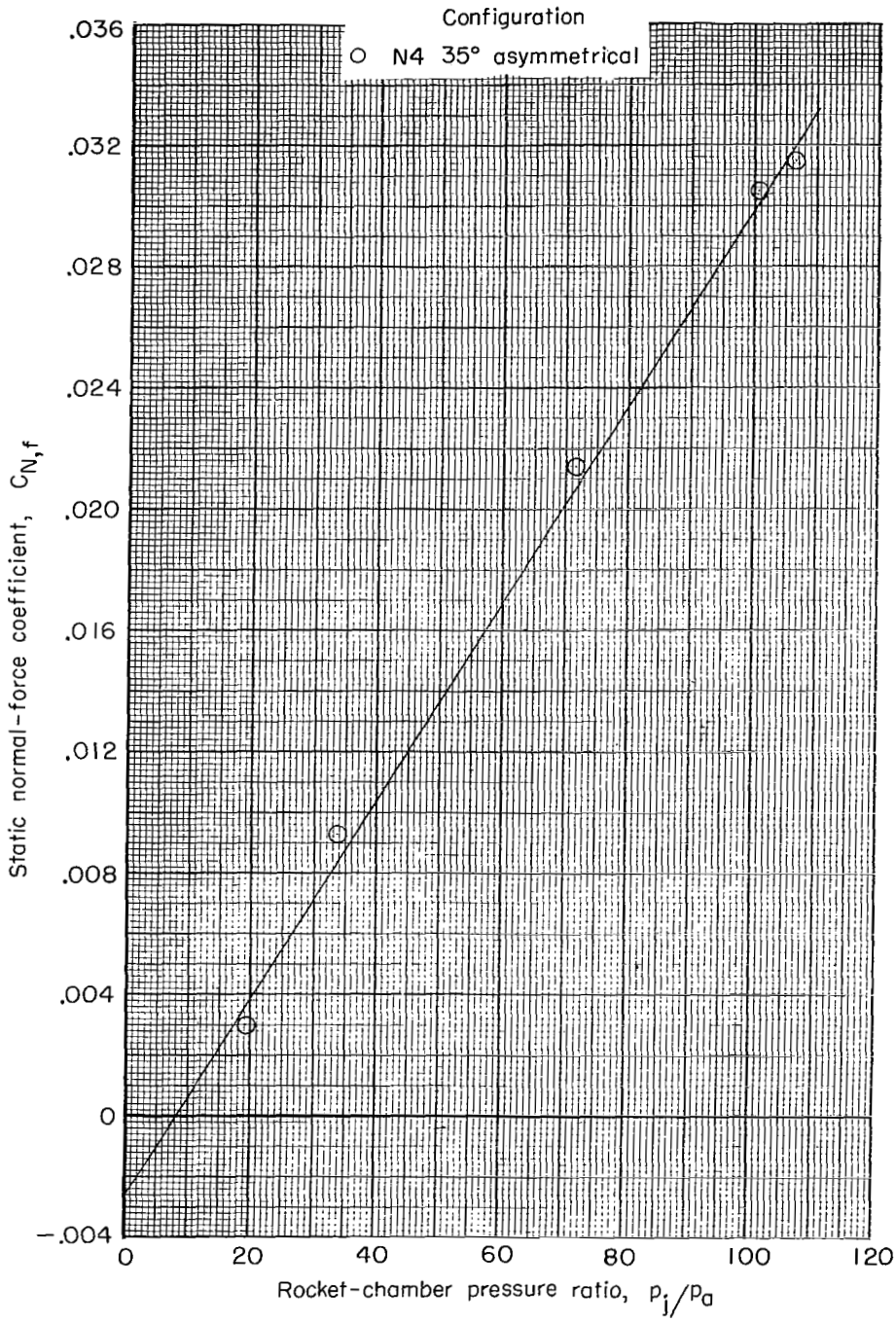

(b) Variation of normal-force coefficient with rocket-chamber pressure ratio.

Figure 6.- Continued.

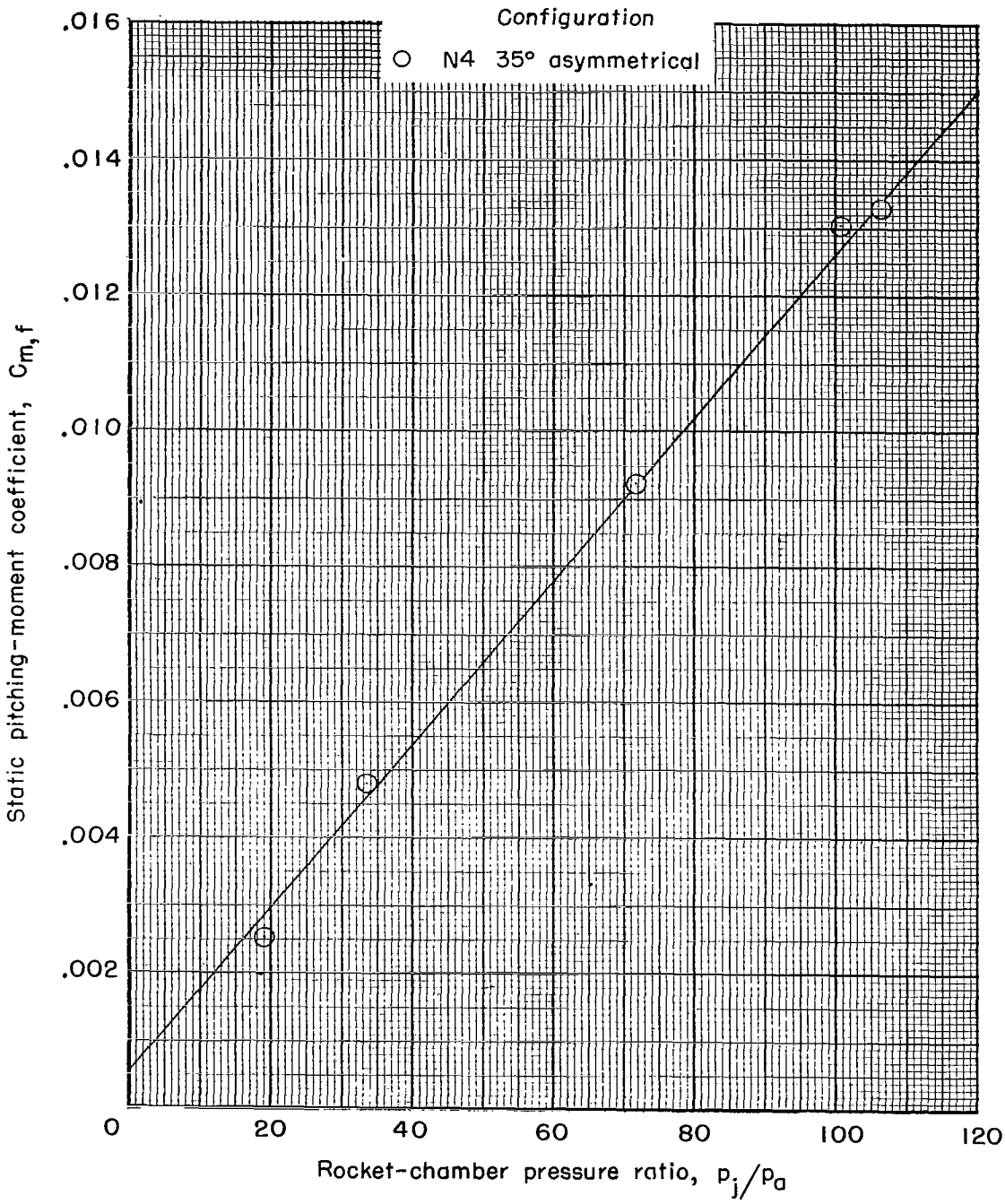

(c) Variation of pitching-moment coefficient about apex with rocket-chamber pressure ratio.

Figure 6.- Concluded.

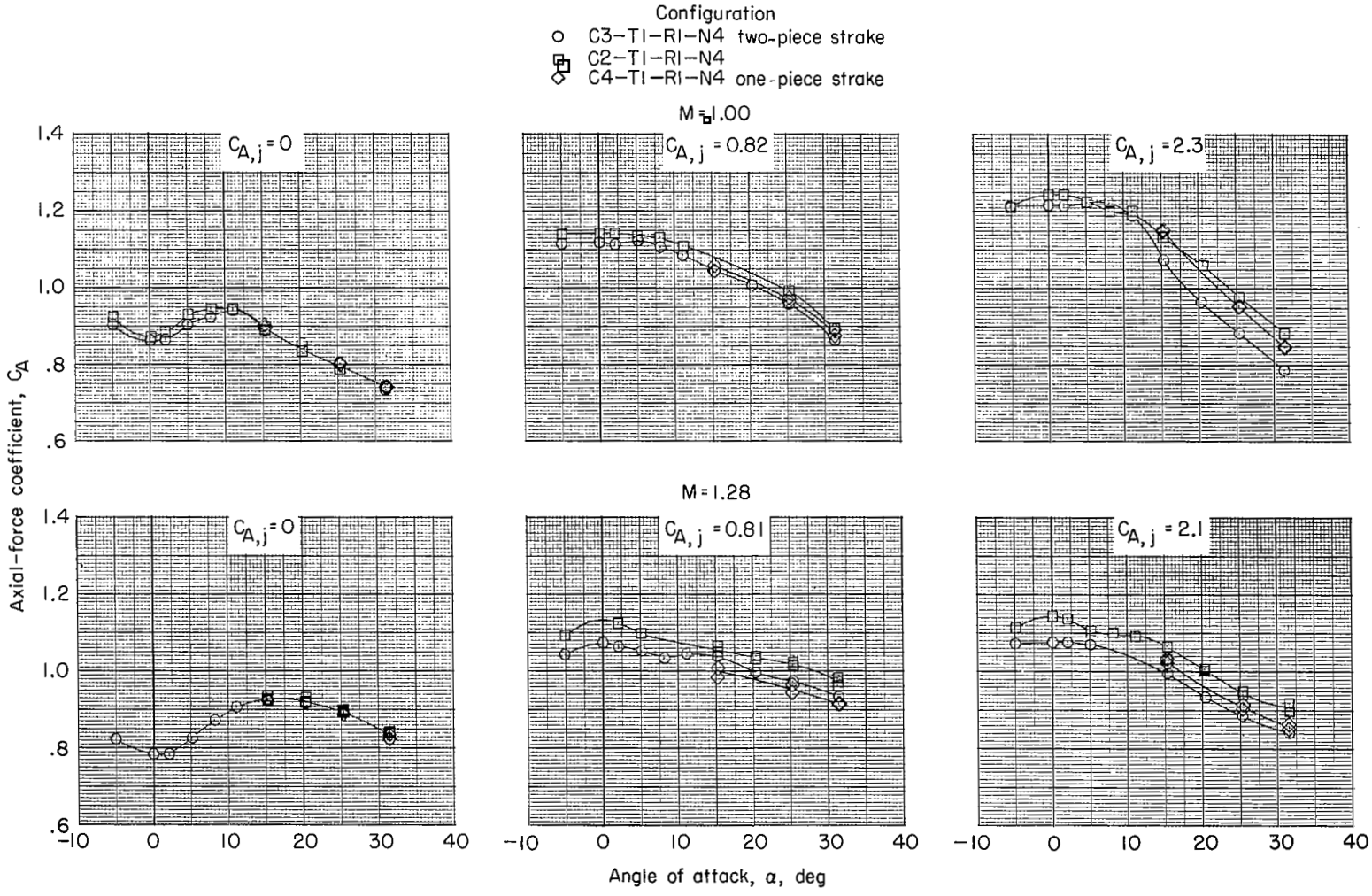

(a) Axial-force coefficient.

Figure 7.- Effect of antenna and strakes on axial-force, normal-force, and pitching-moment coefficients for several values of thrust coefficient and Mach number.

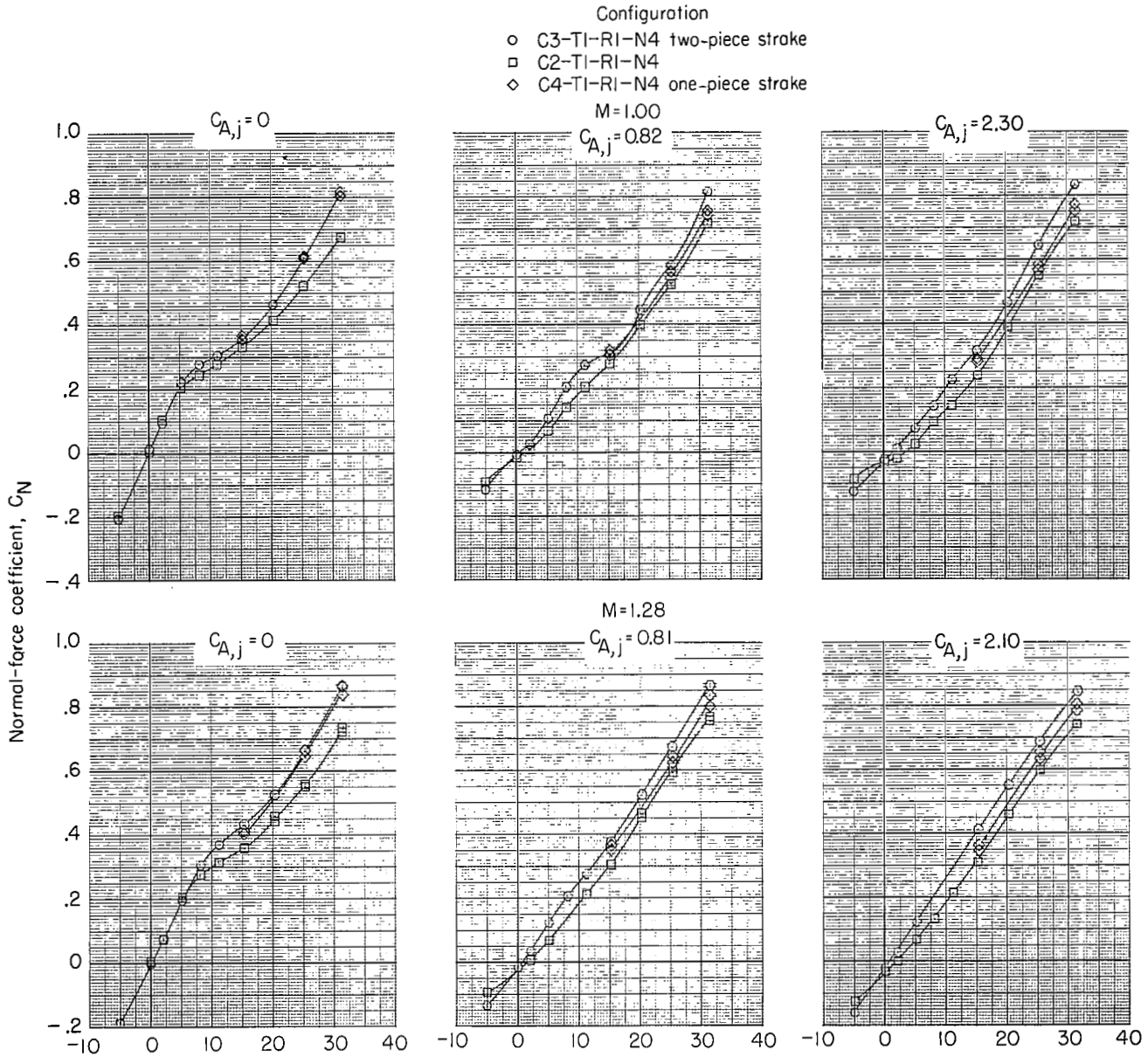

(b) Normal-force coefficient.

Figure 7.- Continued.

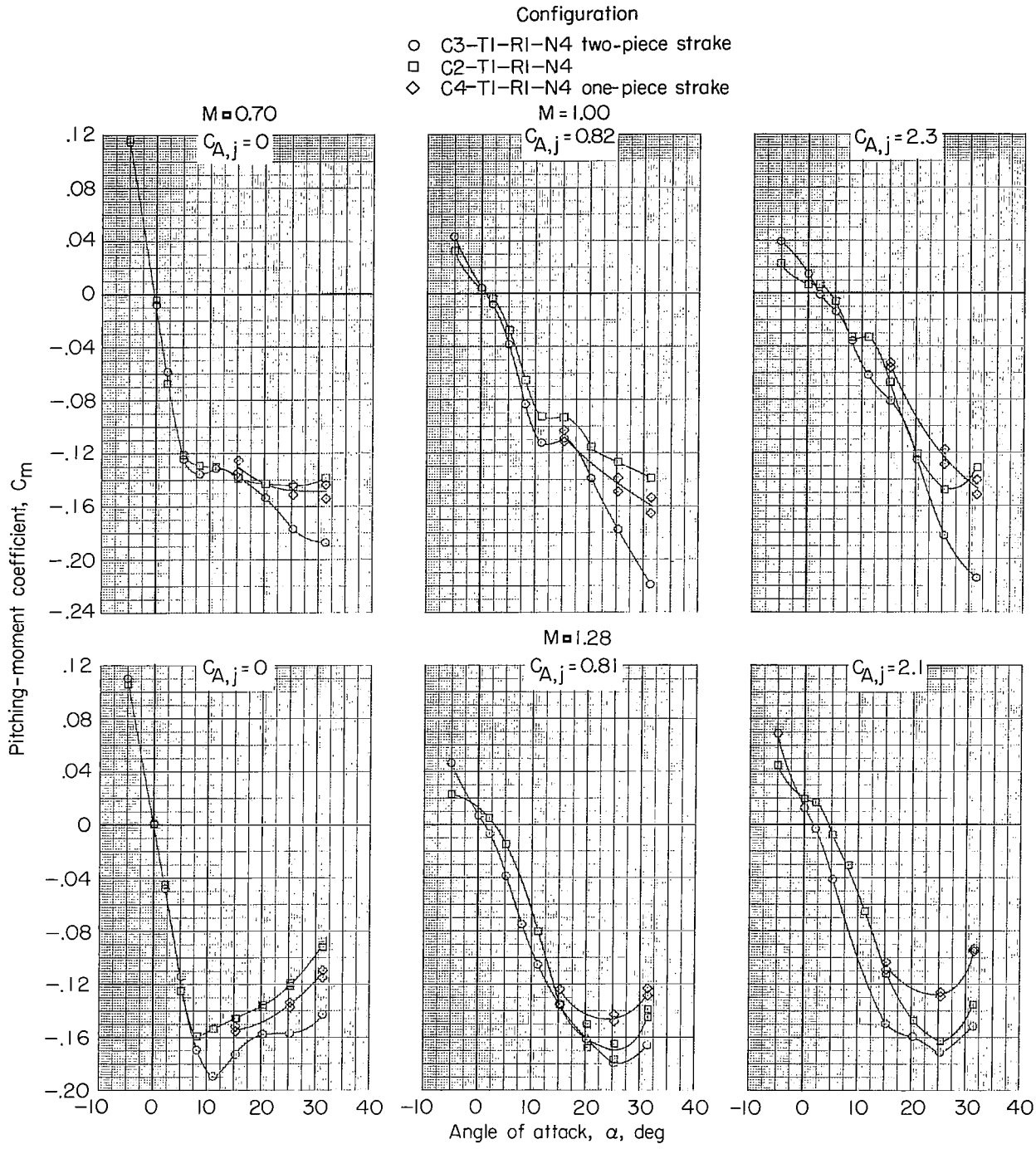

(c) Pitching-moment coefficient.

Figure 7.- Concluded.

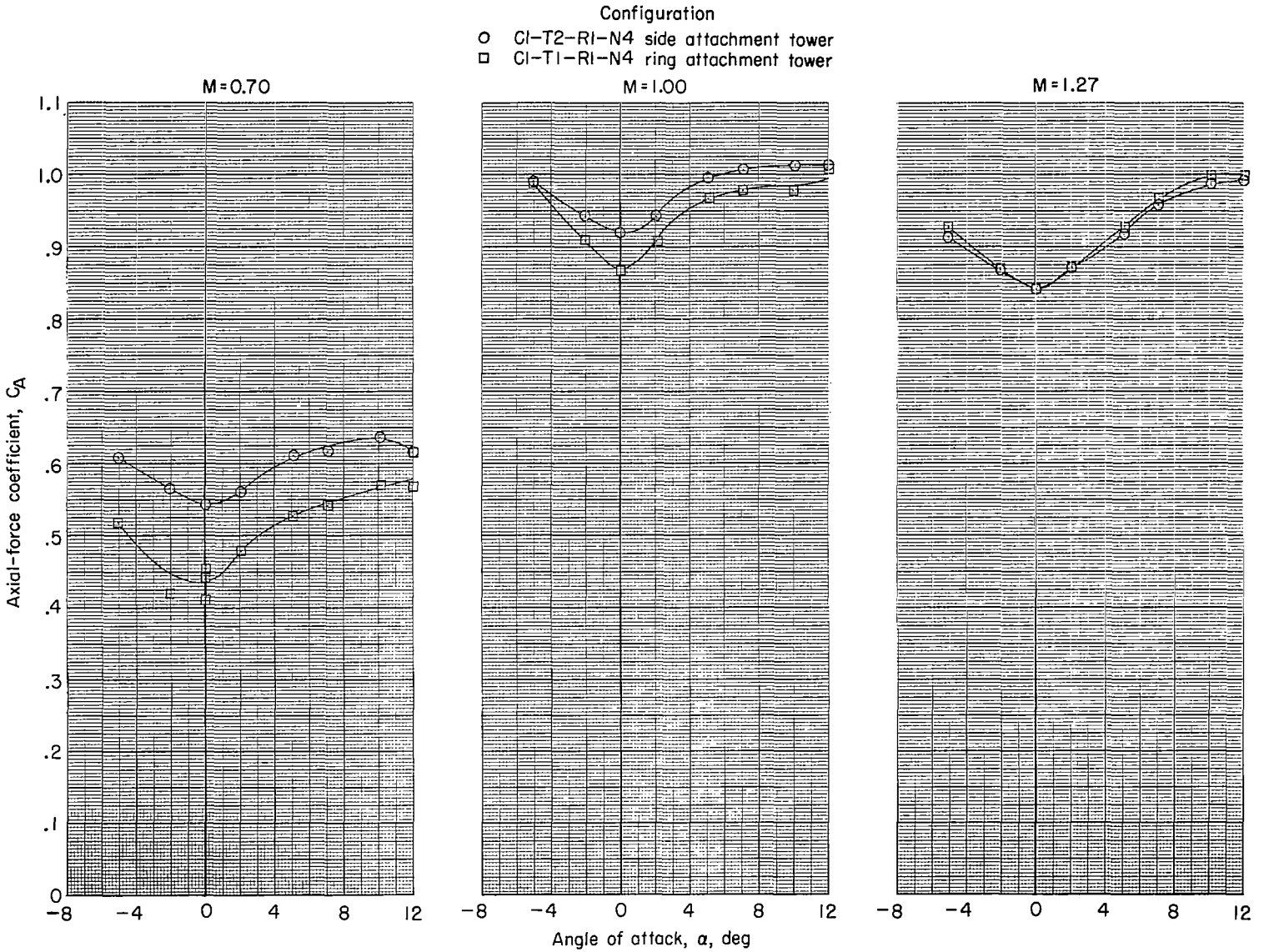

(a) Axial-force coefficient.

Figure 8.- Effect of escape-rocket tower on axial-force, normal-force, and pitching-moment coefficients for several values of Mach number. $C_{A,j} = 0.0$; Skirt disk off.

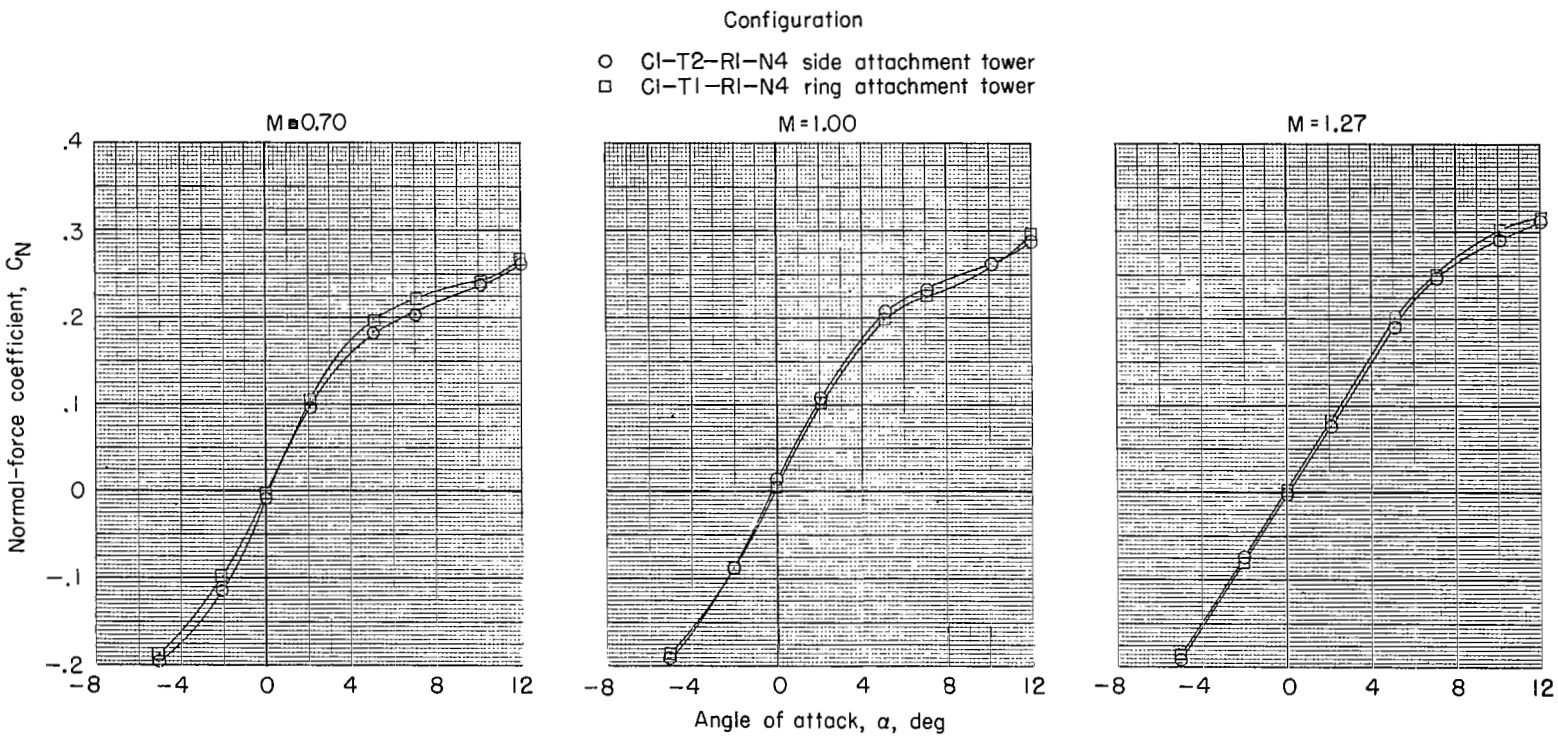

(b) Normal-force coefficient.

Figure 8.- Continued.

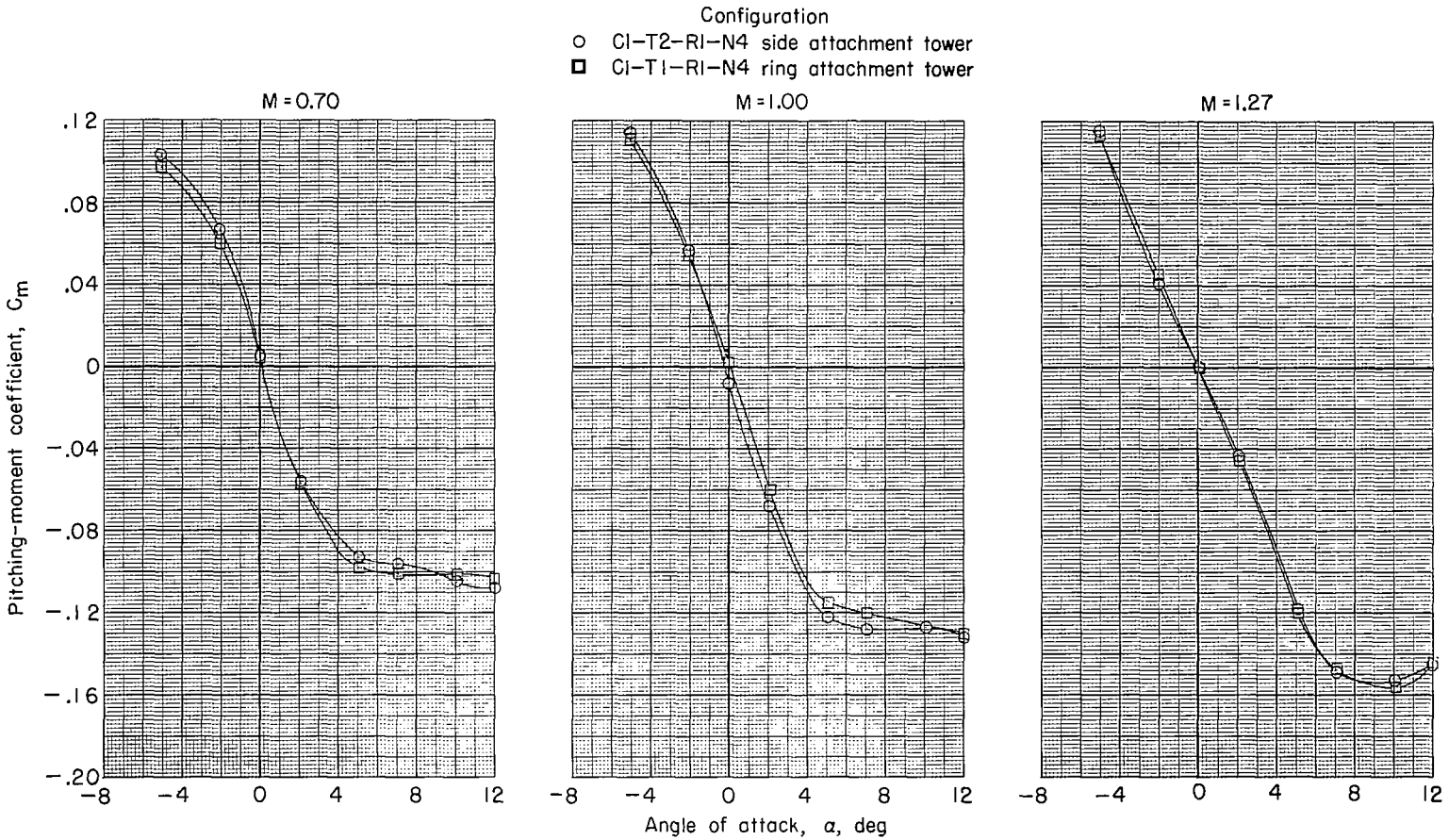

(c) Pitching-moment coefficient.

Figure 8.- Concluded.

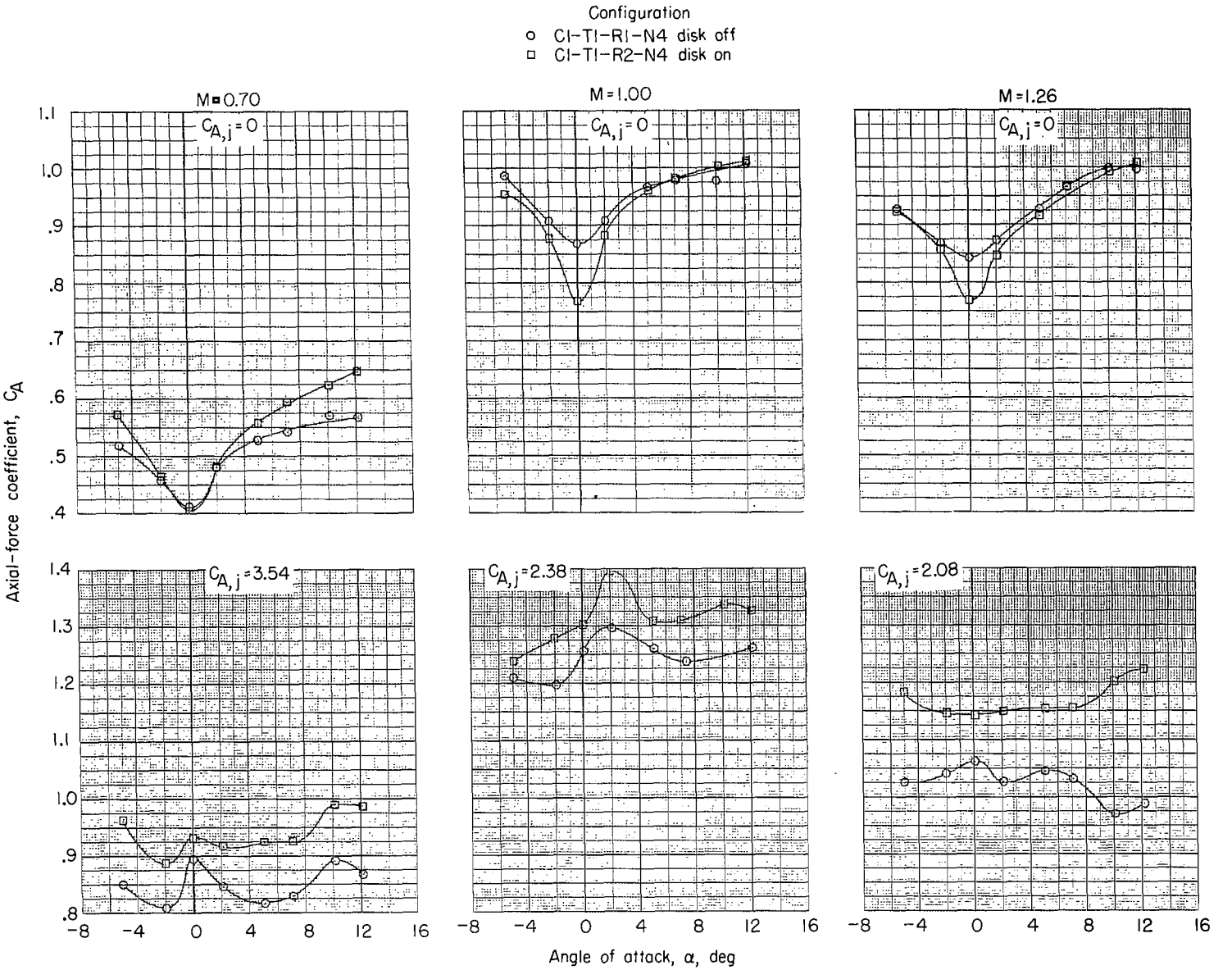

(a) Axial-force coefficient.

Figure 9.- Effect of rocket skirt disk on axial-force, normal-force, and pitching-moment coefficients for several values of Mach number and thrust coefficient. Rocket tower T1.

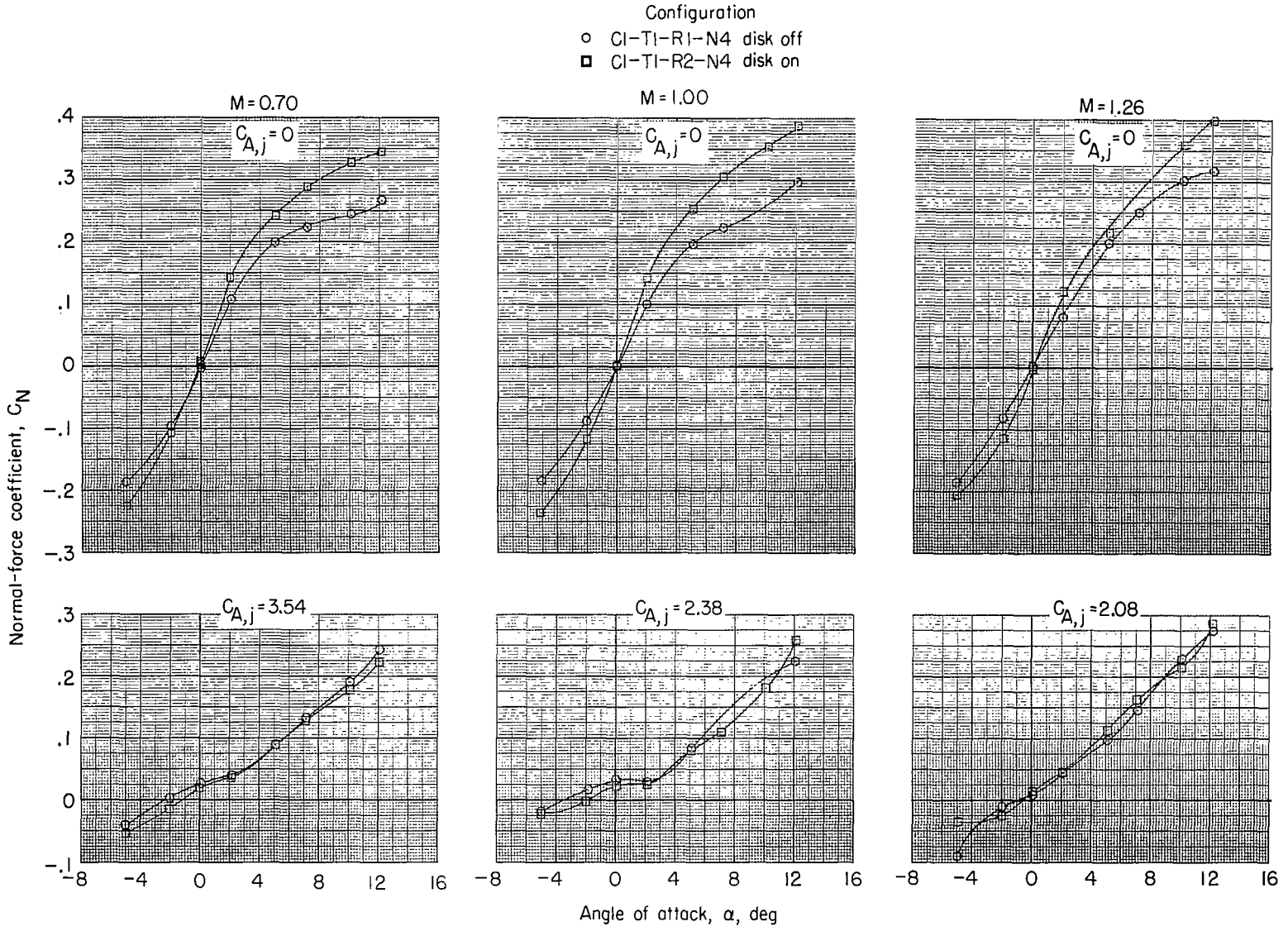

(b) Normal-force coefficient.

Figure 9.- Continued.

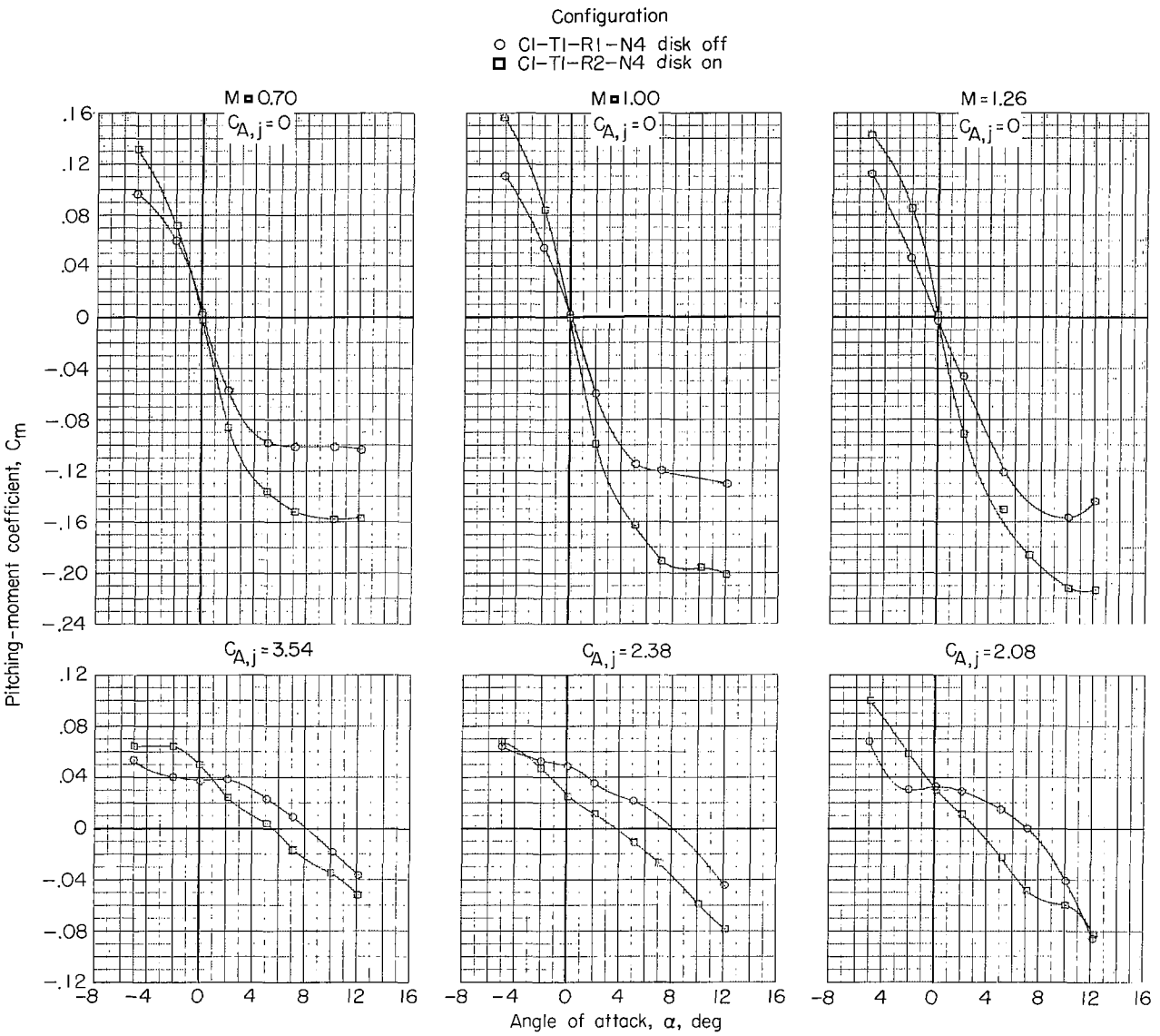

(c) Pitching-moment coefficient.

Figure 9.- Concluded.

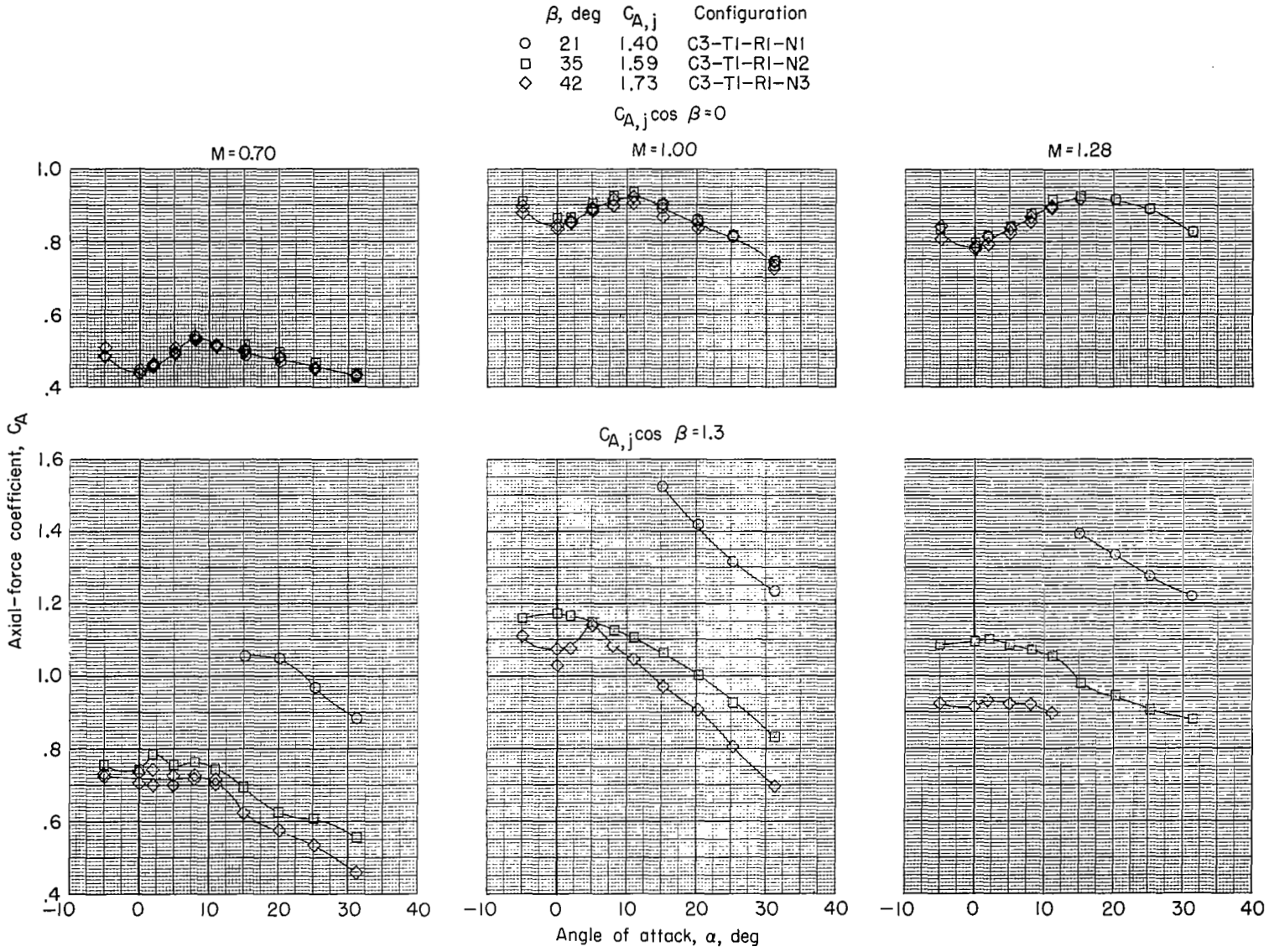

(a) Axial-force coefficient.

Figure 10.- Effect of nozzle cant angle on axial-force, normal-force, and pitching-moment coefficients for several values of $C_{A,j}$ cos β and Mach number.

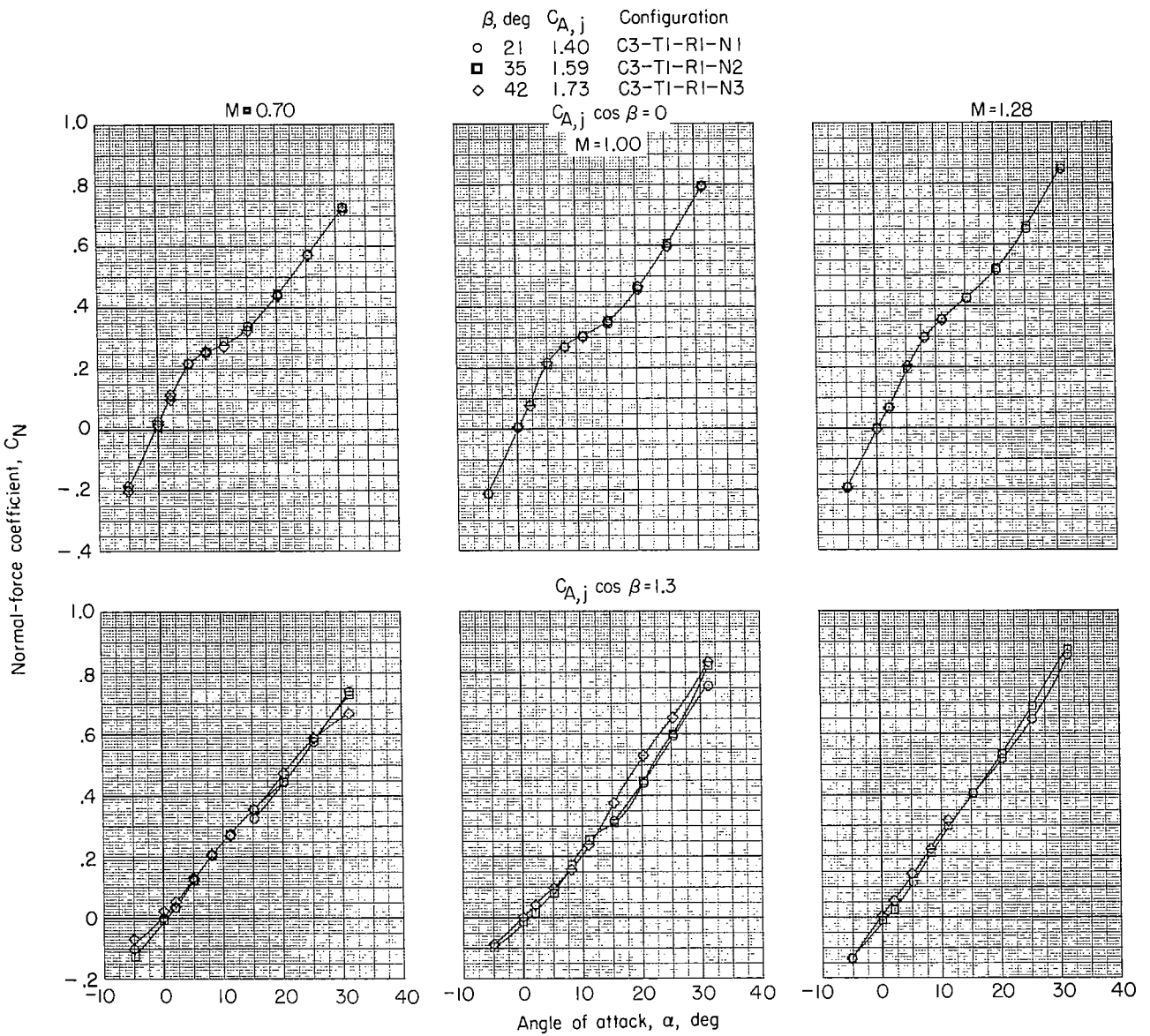

(b) Normal-force coefficient.

Figure 10.- Continued.

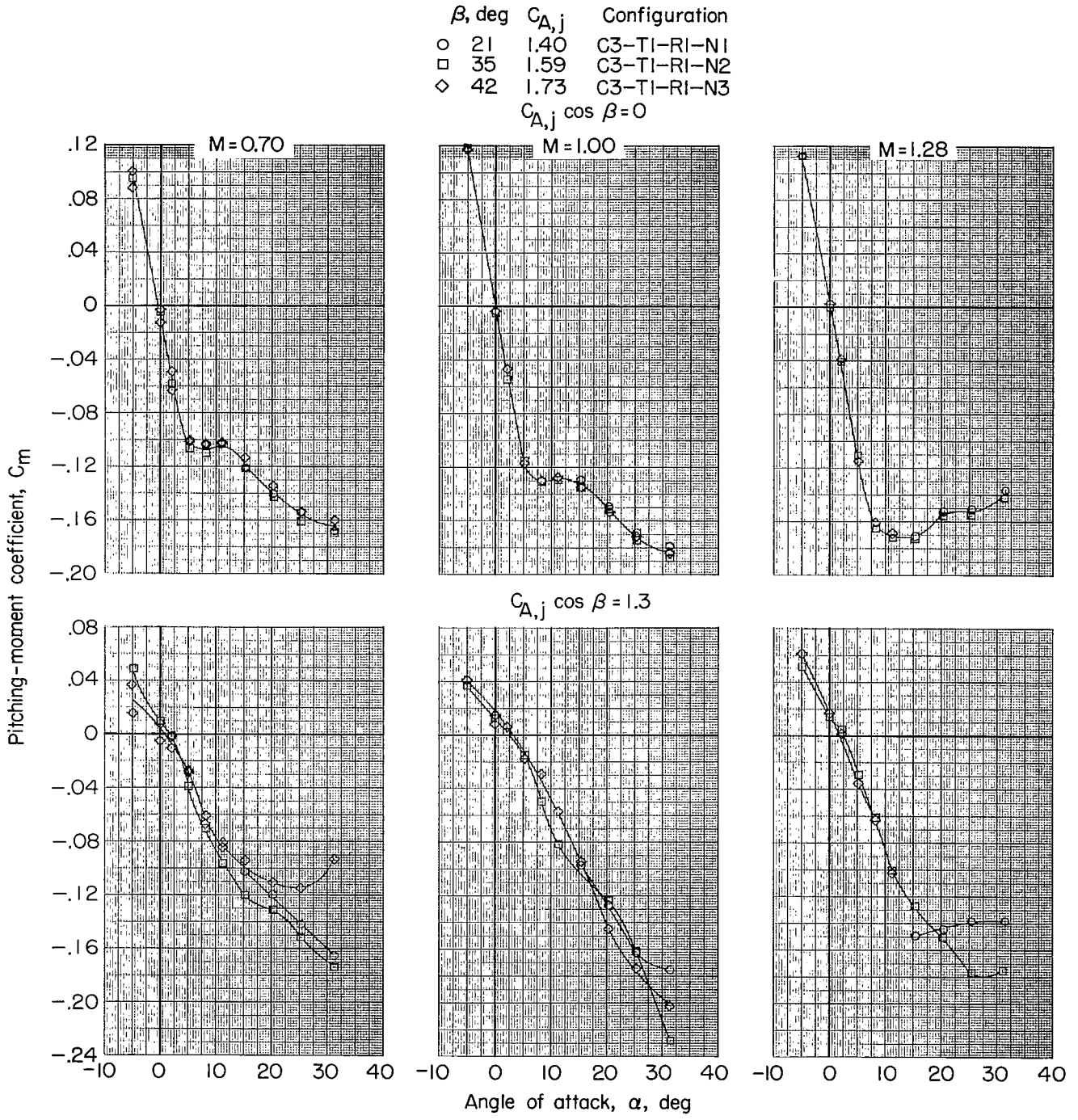

(c) Pitching-moment coefficient.

Figure 10.- Concluded.

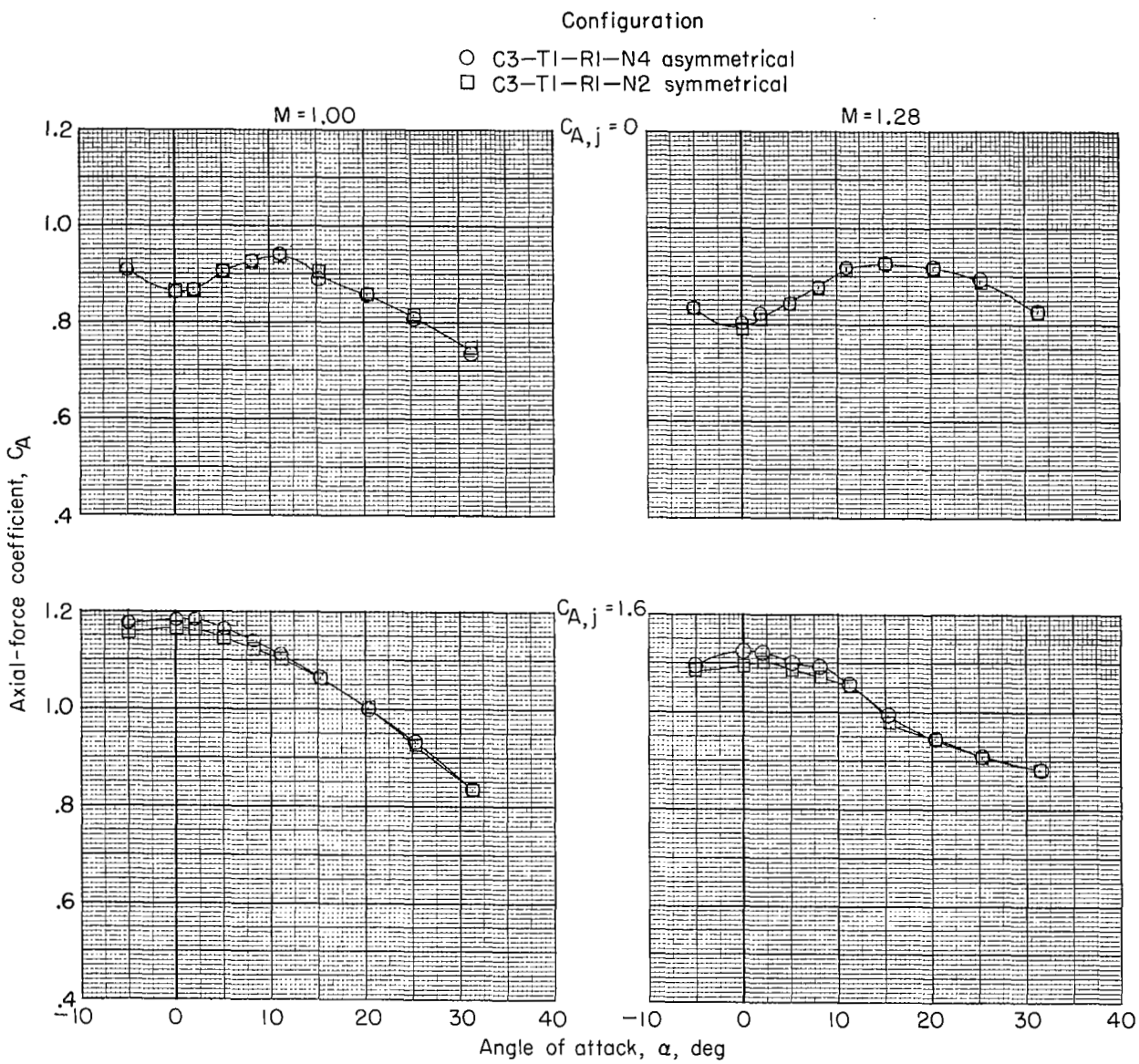

(a) Axial-force coefficient.

Figure 11.- Effect of thrust vector on axial-force, normal-force, and pitching-moment coefficients for several values of thrust coefficient and Mach number.

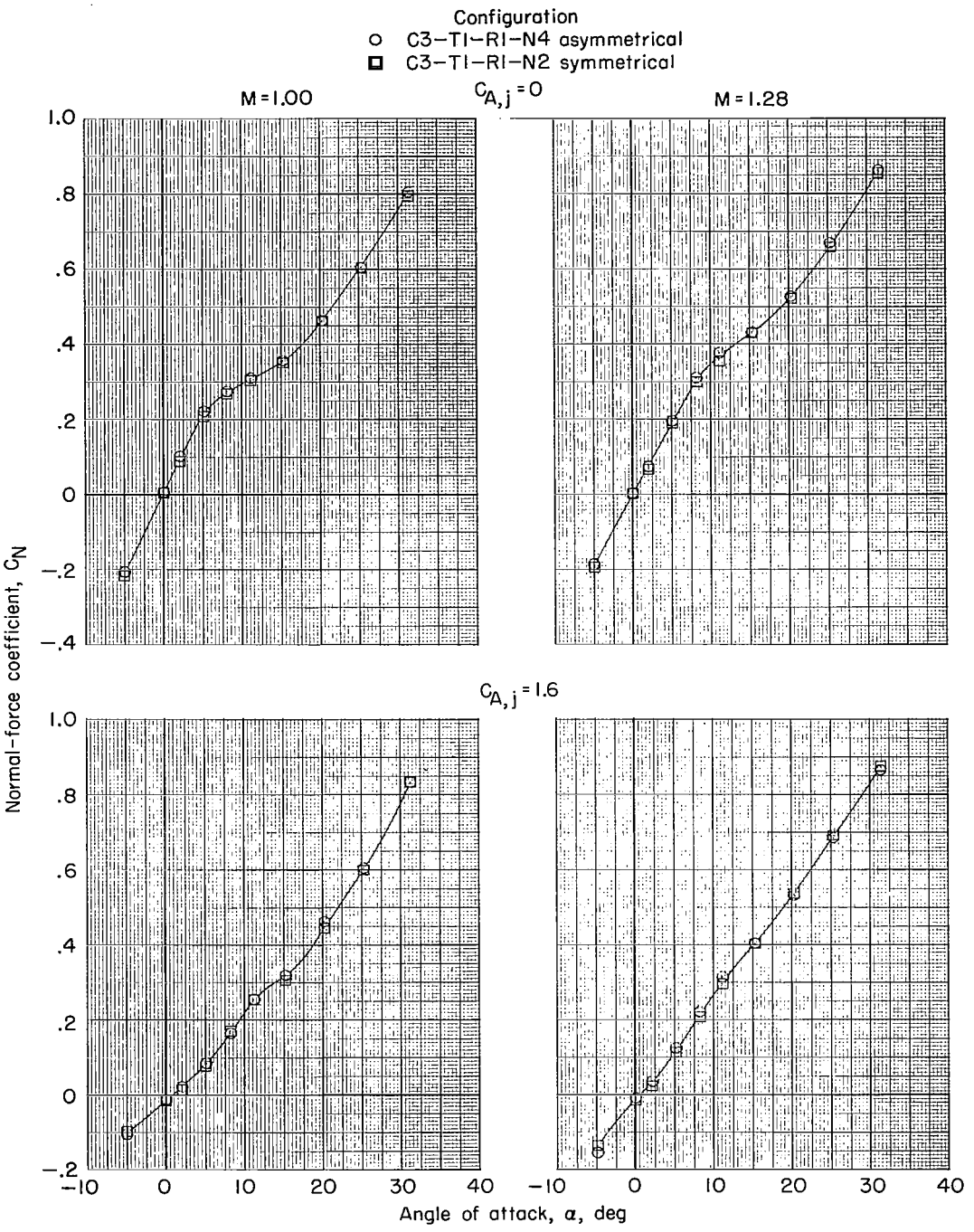

(b) Normal-force coefficient.

Figure 11.- Continued.

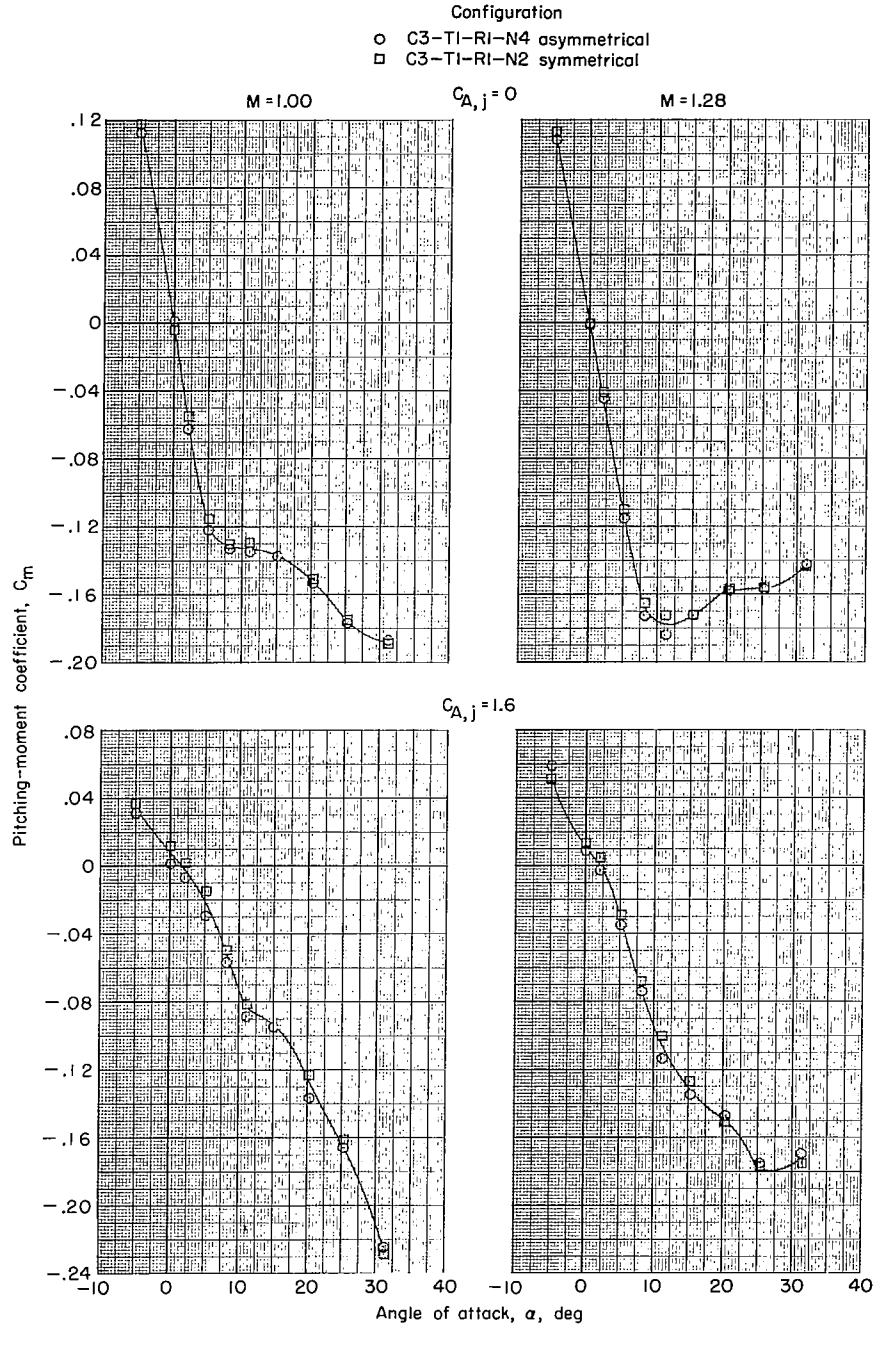

(c) Pitching-moment coefficient.

Figure 11.- Concluded.

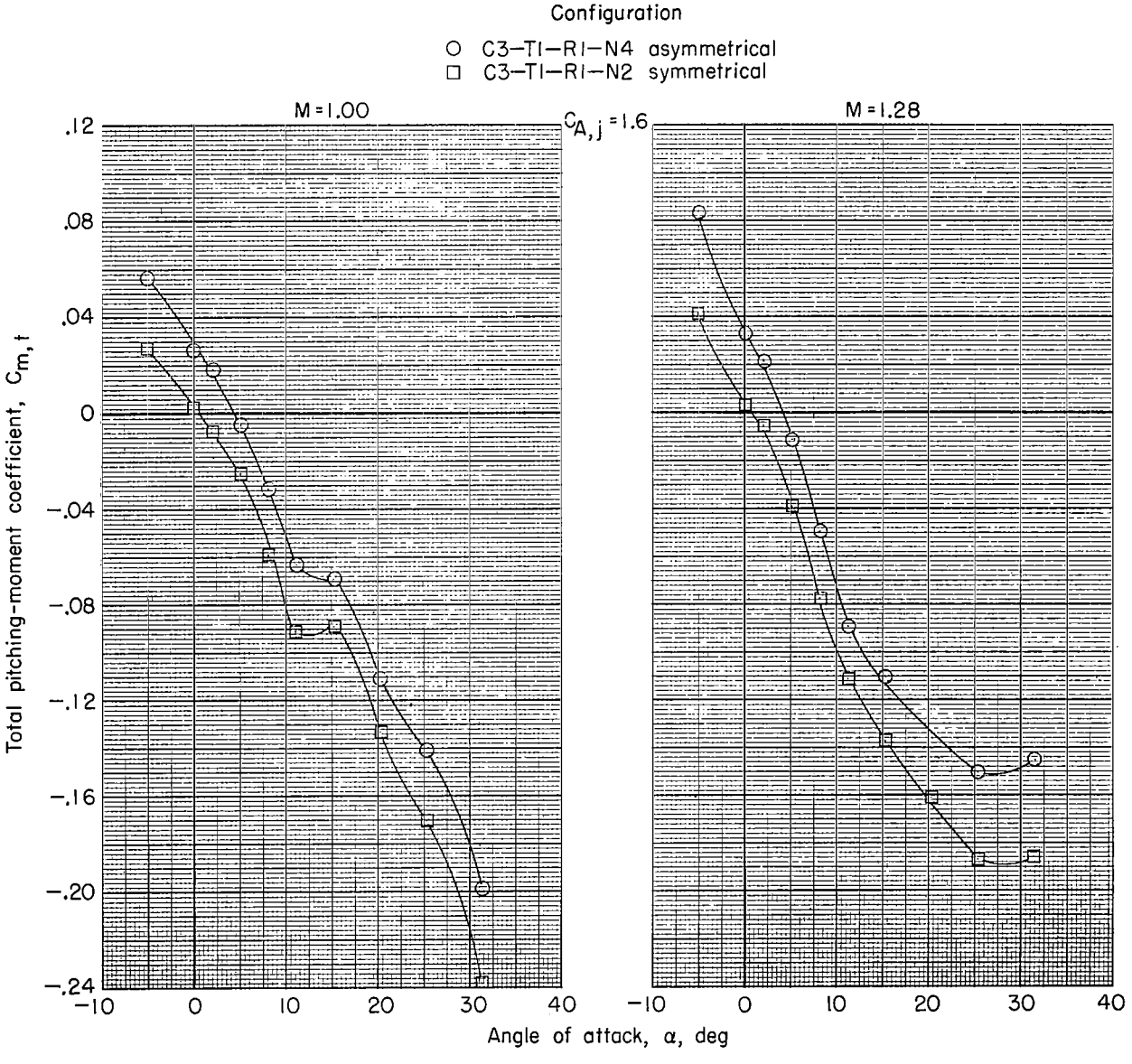

Figure 12.- Effect of thrust vector on total pitching-moment coefficient for two values of Mach number. $C_{A,j}$ = 1.6.

"The aeronautical and space activities of the United States shall be conducted so as to contribute . . . to the expansion of human knowledge of phenomena in the atmosphere and space. The Administration shall provide for the widest practicable and appropriate dissemination of information concerning its activities and the results thereof."

—NATIONAL AERONAUTICS AND SPACE ACT OF 1958

NASA SCIENTIFIC AND TECHNICAL PUBLICATIONS

TECHNICAL REPORTS: Scientific and technical information considered important, complete, and a lasting contribution to existing knowledge.

TECHNICAL NOTES: Information less broad in scope but nevertheless of importance as a contribution to existing knowledge.

TECHNICAL MEMORANDUMS: Information receiving limited distribution because of preliminary data, security classification, or other reasons.

CONTRACTOR REPORTS: Scientific and technical information generated under a NASA contract or grant and considered an important contribution to existing knowledge.

TECHNICAL TRANSLATIONS: Information published in a foreign language considered to merit NASA distribution in English.

SPECIAL PUBLICATIONS: Information derived from or of value to NASA activities. Publications include conference proceedings, monographs, data compilations, handbooks, sourcebooks, and special bibliographies.

TECHNOLOGY UTILIZATION PUBLICATIONS: Information on technology used by NASA that may be of particular interest in commercial and other non-aerospace applications. Publications include Tech Briefs, Technology Utilization Reports and Notes, and Technology Surveys.

Details on the availability of these publications may be obtained from:

SCIENTIFIC AND TECHNICAL INFORMATION DIVISION

NATIONAL AERONAUTICS AND SPACE ADMINISTRATION

Washington, D.C. 20546